

Mechanistic Insights into Alkene Chain Growth Reactions Catalyzed by Nickel Active Sites on Ordered Microporous and Mesoporous Supports

Journal:	Catalysis Science & Technology
Manuscript ID	CY-MRV-06-2020-001186.R2
Article Type:	Minireview
Date Submitted by the Author:	24-Aug-2020
Complete List of Authors:	Joshi, Ravi; Purdue University, Chemical Engineering Saxena, Arunima; Purdue University, Chemical Engineering Gounder, Rajamani; Purdue University, Chemical Engineering

SCHOLARONE™ Manuscripts

MINI REVIEW

Received 00th June 2020, Accepted 00th June 2020

DOI: 10.1039/x0xx00000x

Mechanistic Insights into Alkene Chain Growth Reactions Catalyzed by Nickel Active Sites on Ordered Microporous and Mesoporous Supports

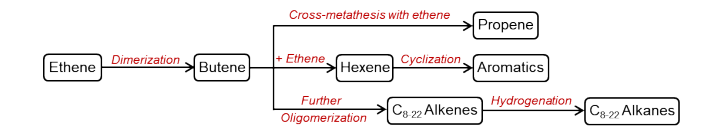
Ravi Joshi, Arunima Saxena and Rajamani Gounder*

Alkene oligomerization on heterogeneous Ni-based catalysts has been studied for several decades, with recent attention focused on the preparation, structure and function of Ni active site motifs isolated within microporous and mesoporous supports, including zeolites and metal-organic frameworks (MOFs). This mini-review focuses on the active site requirements and the microscopic kinetic and mechanistic details that become manifested macroscopically as activation and deactivation behavior during oligomerization catalysis, and that determine measured reaction rates and selectivity among alkene isomer products. The preponderance of mechanistic evidence is consistent with the coordination-insertion (Cossee-Arlman) cycle for alkene oligomerization prevailing on heterogeneous Ni-exchanged zeolites and MOFs, even when external co-catalysts are not present, as they often are in homogeneous Ni-based oligomerization catalysis. Certain mechanistic features of the coordination-insertion route allow catalyst and active site design strategies to influence product selectivity. Our mini-review provides a critical discussion of reported alkene oligomerization data and the challenges in their measurement and interpretation, and concludes with an outlook for future research opportunities to improve our kinetic and mechanistic understanding of alkene chain growth chemistries mediated by Ni-based porous catalysts.

1. Introduction

Alkene oligomerization on heterogeneous Ni-based catalysts has been studied for several decades, 1-3 with renewed interest in the past decade as the petrochemical industry has responded to the cheap and abundant supply of light alkane feedstocks found in U.S. and global shale gas reserves. Shalegas derived ethane has replaced crude-derived naphtha as the preferred feedstock for steam cracking processes in certain locations, with planned increases to global ethane steam cracking capacity. Using ethane as a feedstock for steam cracking predominantly produces ethene (~75% of cracker output),4 but produces less of the heavier co-products such as propene, butenes, and aromatics (benzene, toluene, and xylene; BTX) as compared to naphtha feedstocks. Thus, the relative abundance of ethene within cracker product streams creates new opportunities to further convert them to produce the deficit heavier co-products. Also, efforts to decarbonize the transportation sector have focused on producing renewable middle-distillate fuels to power the freight and aviation segments, which are more difficult to electrify than light duty passenger vehicles. Research in this area has focused on chemistries and processes for converting biomass-derived ethanol into middle-distillate fuels, which also involve ethene and other light alkenes as key intermediates.⁵ As a result,

opportunities exist to convert ethene and other light alkenes derived from shale-gas condensates or biomass-based alcohols into higher value hydrocarbons by chemical pathways that involve alkene chain growth chemistries, as shown for the case of ethene in Scheme 1. Light alkene dimers are important chemical intermediates in alkylation processes that produce premium blendstocks for gasoline, and in cross-metathesis processes to produce oligomers of chain lengths that are nonintegral multiples of reactant monomers, as often valued as comonomers in polymerization. Selective formation of alkene trimers generates intermediates that can undergo cyclization to make aromatic compounds, while even further oligomerization produces long-chain alkenes that can be hydrogenated to produce paraffinic blendstocks for middle-distillate fuels. Alkene chain growth chemistries are thus integral components of routes to convert light alkenes into chemical intermediates and hydrocarbon blendstocks for transportation fuels.



Scheme 1 Pathways for converting ethene to chemicals and middle-distillate fuels.; analogous schemes can be drawn for other alkene reactants.

Nickel is particularly useful as a catalytic element in alkene chain growth reactions, known since the discovery of the "nickel effect" in Karl Ziegler's lab, wherein accidental traces of Ni

Charles D. Davidson School of Chemical Engineering, Purdue University, 480 Stadium Mall Drive, West Lafayette, IN 47907, USA. E-mail: rgounder@purdue.edu

organic salts during the reaction of ethene with triethylaluminum (Aufbau reaction) formed butene instead of trialkylaluminum compounds with long alkyl chains.^{6, 7} The discovery of the "nickel effect" led to the development of organonickel chemistries to form carbon-carbon bonds, including alkene dimerization and oligomerization.8 Ni organometallic complexes favor chain termination over propagation,9 and are thus more selective towards alkene dimerization than oligomerization compared to organometallic complexes of other transition metals (Ti, Ta, Zr, Cr). 10-14 Yet, Ni complexes can form trimer and tetramer products by codimerization between product and reactant alkenes, 15, 16 at ratios that depend on the ligands coordinated to the Ni center.8, 9, 17 Homogeneous Ni-based catalysts are used in industrial processes such as IFP Dimersol, 18, 19 Shell Higher Olefins Process,8, 20 and UOP Linear-1 because of their high reactivity and relatively low cost compared to other homogeneous organometallic complexes.21

There are no industrial processes using heterogeneous Ni catalysts for alkene oligomerization, to the best of our knowledge, although solid acid catalysts such as ZSM-5 have been used in the MOGD (Mobil Olefins to Gasoline and Distillate) process to oligomerize C₃ and C₄ alkenes.²² At low temperatures (<573 K) similar to that of the MOGD process, solid acid catalysts exhibit much lower oligomerization rates for ethene than for C₃-C₄ alkene reactants, reflecting the less stable primary carbenium ions or alkoxides²³ compared to their secondary and tertiary counterparts;^{24, 25} higher temperatures favor aromatization, transfer hydrogenation and cracking reactions over oligomerization. The development of heterogeneous Ni catalysts for oligomerization is motivated by the ability of homogeneous Ni catalysts to exhibit high reactivity and selectivity for ethene dimerization and oligomerization at lower temperatures, and O'Connor and Kojima¹ have reviewed the developments in heterogeneous Ni catalysts until 1990. Since then, considerable research efforts have focused on materials synthesis approaches to prepare Ni active sites exchanged onto heterogeneous microporous and mesoporous supports, including zeolites and metal-organic frameworks (MOFs), developing characterization techniques to interrogate the structure of Ni-exchanged porous materials, and establishing relationships between the active site and support structures on catalytic rate and selectivity behavior.

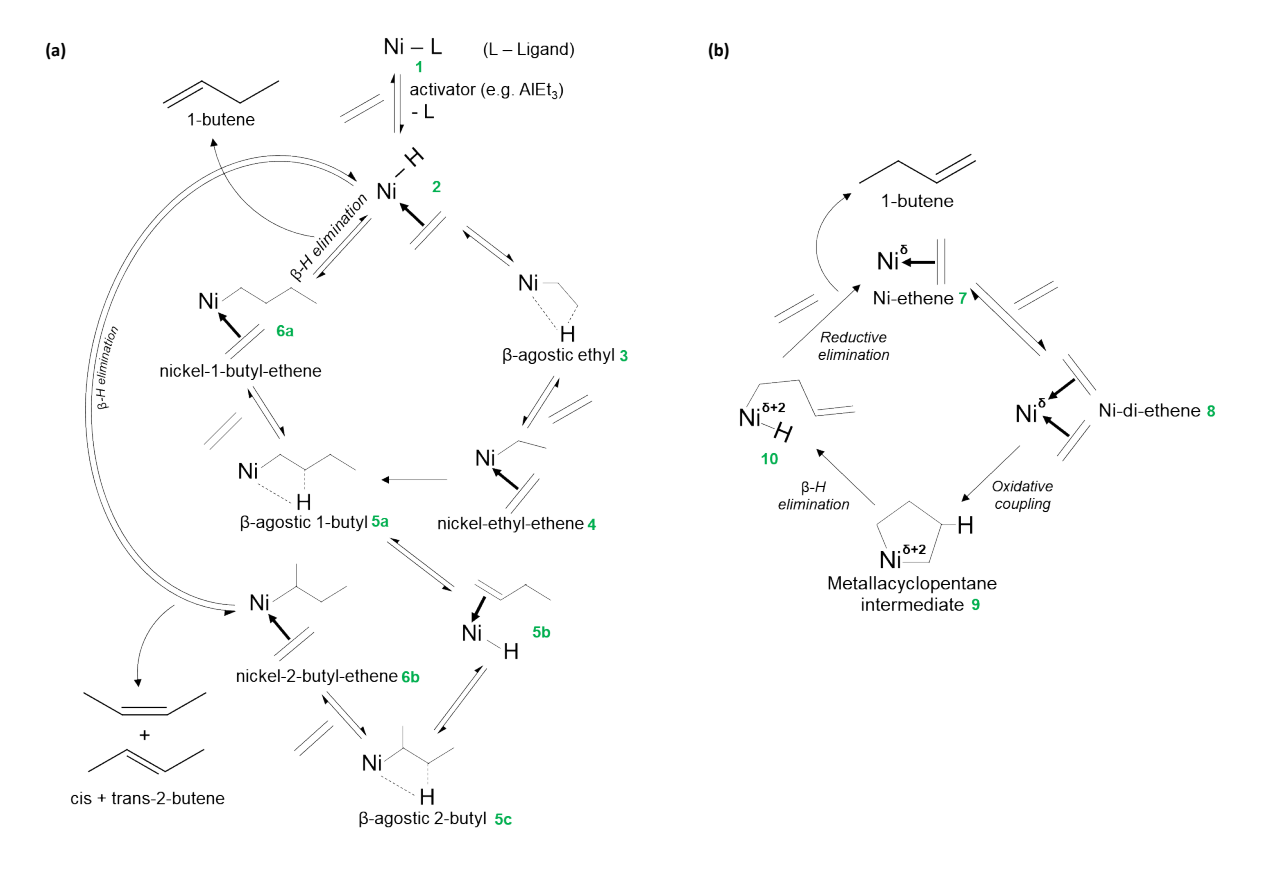
Recent reviews related to this topic have focused on: (i) the structure of Ni active sites in inorganic materials and experimental conditions for ethene oligomerization,² (ii) synthesis approaches for preparing Ni catalysts^{14, 26} and evaluating their performance for light alkene oligomerization,¹⁴ (iii) structural details of Ni-based MOFs, reaction mechanisms for ethene oligomerization, and various pathways for converting ethene to chemicals,³ and (iv) the effect of

oligomerization reaction conditions on product distribution and process configurations for commercial-scale applications. 5 The discussion in this mini-review instead focuses on the mechanistic details underlying the observed activation and deactivation behavior, the reaction kinetics, and the product selectivity of Ni-based ordered porous materials for alkene oligomerization. First, we discuss the factors that influence whether co-catalysts need to be supplied externally to initiate alkene oligomerization cycles, which underlies observed catalytic activation phenomena. Next, we discuss how observations of transient deactivation behavior as a function of material properties and reaction conditions can be used to glean insights into potential deactivation mechanisms. We then provide a critical survey of reported alkene oligomerization kinetic data, and discuss challenges associated with their measurement and mechanistic interpretation. We identify mechanistic considerations that influence the molecular structures of the alkene oligomer products formed, and how they depend on material properties and reaction conditions. Finally, we conclude with an outlook for future research opportunities to address gaps in our current understanding of alkene oligomerization catalyzed by Ni-based porous materials.

2. Catalyst activation during alkene oligomerization

Ni-based homogeneous catalysts operate by either the (Cossee-Arlman)²⁷⁻²⁹ coordination-insertion metallacycle^{30, 31} mechanism for alkene chain growth reactions.^{9, 11, 32} Scheme 2a³³ shows the coordination-insertion mechanism at Ni²⁺ active centers, while Scheme 2b³³ shows the metallacycle mechanism at Ni^δ active centers, depicted for ethene dimerization. The coordination-insertion mechanism is initiated by the conversion of the precursor Ni sites into the active sites, Ni(II)-hydride (2, Scheme 2a) or Ni(II)-alkyl species, and generally requires alkyl aluminum, borane or borohydride compounds to replace the ligands on the Ni precursor sites with the hydride or alkyl functional groups. 11, 34, 35 Certain homogeneous Ni catalysts36, 37 can form the active sites for coordination-insertion cycles in situ, via reaction of their ligands with the alkene that allows them to initiate coordinationinsertion cycles in the absence of an external activator. Unlike the coordination-insertion mechanism, the metallacycle mechanism does not involve an activation step because the active site is an alkene-coordinated Ni^δ cation (7, Scheme 2b) that undergoes successive coordination with alkene molecules to form metallacycloalkane intermediates (9, Scheme 2b) by oxidative coupling. As a result, the Ni-based catalysts that operate via the metallacycle mechanism do not require the addition of external co-catalysts or activators.

Mini review



Scheme 2 (a) Coordination-insertion and (b) metallacycle mechanism shown for ethene dimerization (adapted with permission from Joshi et al. 33); the formal oxidation state of Ni is +2 for all intermediates in (a).

The active state of Ni cations on heterogeneous catalysts for alkene chain growth reactions has long been debated, as discussed in detail previously.^{2, 38} Studies predominantly based on electron spin resonance (ESR) spectroscopy have proposed reduction of Ni²⁺ to Ni⁺ cations in zeolites that serve as active sites,³⁹⁻⁴⁴ although structures for Ni²⁺ cations are silent in EPR spectroscopy using the conventional microwave frequencies used in these studies.⁴⁵ In contrast, more recent studies using CO infrared spectroscopy have shown Ni⁺ cations to behave as spectator species,⁴⁶⁻⁴⁸ and *in-situ* X-ray absorption studies^{33, 49} have shown Ni cations to be predominantly present in +2 oxidation during the alkene chain growth reactions. Thus, the mechanistic discussion that follows is focused predominantly on Ni²⁺-based active site structures.

2.1 Mechanisms of Ni activation on microporous and mesoporous inorganic supports

Alkene oligomerization on isolated nickel sites (Ni²⁺) supported on porous inorganic materials, such as zeolites and mesoporous materials, has been shown to proceed via the coordination-insertion (i.e., Cossee-Arlman) mechanism.^{33, 38} Other catalysts that oligomerize alkenes via the coordination-insertion mechanism, such as homogeneous α -diimine Ni compounds^{9, 50, 51} and Ni-based metal organic frameworks (MOFs)^{52, 53}, often require the addition of co-catalysts or activators that form Ni(II)-alkyl (**3**, Scheme 2a) species *in situ* to initiate the catalytic cycles. Yet, such oligomerization cycles can

be initiated on Ni-based porous inorganic materials in the absence of externally supplied co-catalysts,² which can be manifested as an activation period observed during initial reaction times.^{33, 49} Thus, research efforts have focused on determining the kinetic and mechanistic details responsible for converting precursor Ni structures (e.g., Ni²⁺) to reactive intermediates involved in the coordination-insertion cycle (e.g., Ni(II)-alkyI).

Several experimental studies have focused on studying the initiation mechanism of Ni-zeolites of different framework topology, which can influence the coordination environment and location of the Ni sites. Prior to alkene exposure, Ni-zeolites are typically subjected to an inert or oxidative pretreatment (573-803 K, 0-20% O₂), after which they contain isolated Ni²⁺ cations present in a distorted tetrahedral geometry. 33, 46, 47, 49 Ni-exchanged X zeolites, after being subjected to an oxidative pretreatment (773 K, 20% O₂) and subsequent reaction with propene (453 K), showed an induction period in the measured propene consumption rate (453 K).⁴⁹ This induction period was observed to become shorter with increasing reaction temperature (453-493 K), but remained largely unaffected by variation in propene pressure.⁴⁹ This observation led the authors to suggest that the induction period in propene consumption rate reflected the migration of Ni²⁺ cations from the double six-membered rings (D6R) of FAU to the sodalite cages, because equivalent experiments on Ni-MOR and Ni-SiO₂ materials that do not contain D6R did not show such an

induction period.⁴⁹ Subsequent studies, however, reported an induction period for ethene oligomerization (453 K) on Ni-Beta zeolites that do not contain D6R units, although induction periods were only observed at low ethene partial pressures (<0.004 bar C_2H_4).³³ These findings highlight how the conclusions derived from experimental investigations of the *in situ* formation of active sites depend on the choice of reaction conditions used (e.g., alkene pressure), especially if they cause the kinetics of initiation steps to be sufficiently fast to avoid detection. They also indicate that Ni cation migration within different voids of porous supports cannot be the sole mechanistic reason for the induction periods observed during alkene oligomerization.

Experimental findings demonstrate that, in the absence of externally supplied activators, reactant alkenes and co-fed H_2 can assist in forming Ni-hydride or Ni-alkyl intermediates *in situ*. The induction period (i.e., the duration of the activation transient) decreased with increasing ethene partial pressure (0.0005–0.0040 bar C_2H_4) on Ni-Beta, implicating etheneassisted formation of the active sites *in situ*.³³ Furthermore, the induction period on Ni-Beta (<0.0040 bar C_2H_4) was eliminated by co-feeding H_2 to form Ni-hydride intermediates, as evidenced by isotopic H_2 - D_2 scrambling and H/D exchange experiments (453 K), indicating that the kinetics of ethene reacting with Ni²⁺ precursor sites to form Ni(II)-hydride or Ni(II)-alkyl are responsible for the observed induction periods.³³

An operando infrared study⁵⁴ of Ni-Beta (0.015 bar C₂H₄) while increasing the temperature from 173-393 K showed the appearance of an IR peak at 1814 cm-1 (at 173 K) purportedly assigned to a [Ni(II)-H]+ species; gaseous butene products were first detected at 240 K, concomitant with the appearance of IR peaks (3015, 1411, 1602 cm⁻¹) for ethenyl (vinyl, CH₂=CH-) species. The intensities for the IR peaks for [Ni(II)-H]+ and ethenyl species increased with temperature and reached a maximum intensity at 269 K, followed by a gradual decrease in intensity as the temperature was increased to 328 K, before finally disappearing at temperatures above 328 K with the concomitant increase in butene formation rate exponentially with temperature (>328 K).54 The spectral assignment for the [Ni(II)-H]+ species was based on the observation that an equivalent experiment with deuterated ethene did not show the 1814 cm⁻¹ peak,⁵⁴ however, spectral data in the low wavenumber (<1300 cm⁻¹) range was not presented and therefore a corresponding feature for a [Ni(II)-D]+ species, expected around 1288 cm⁻¹ (from isotopic shift calculations) could not be verified. Nevertheless, these observations would be consistent with [Ni(II)-ethenyl]+ and [Ni(II)-H]+ species as intermediates in the coordination-insertion cycle. These authors, however, interpret ethenyl (CH₂=CH⁻) and hydride (H⁻) functional groups to be present on the same Ni species, and propose a redox (+2, +4) catalytic cycle that combines the active site formation and ethene dimerization,⁵⁴ in contradiction to in situ X-ray absorption studies33, 49, 55 that showed the sole presence of Ni(II) during alkene oligomerization catalysis. Additionally, this operando IR study⁵⁴ indicated the formation of a bound acetylenic species (2164 cm⁻¹) at 173 K, which remained detectable as the temperature was increased to 248 K and H_2 was concomitantly formed, but not above this temperature as ethane (>248 K) and butane (>293 K) were detected in the gas phase;⁵⁴ the role of these species in forming coordination-insertion active sites or completing dimerization turnovers remains unclear.

formation of [Ni(II)-ethenyl]⁺ and [Ni(II)-H]⁺ intermediates during the induction period is also supported by density functional theory (DFT) calculations using a BEEF-vdW functional for Ni²⁺ species in the AFI framework. Scheme 3a³⁸ shows the DFT-calculated reaction pathway for the formation of coordination-insertion active sites starting with ionexchanged Ni2+ structures. First, two ethene molecules coordinate to a Ni²⁺ cation (Step 1, Scheme 3a), followed by deprotonation of one ethene to generate a H+ site on the zeolite framework and a [Ni(II)-ethenyl-ethene]+ intermediate (Step 2, Scheme 3a), consistent with operando IR data.⁵⁴ This intermediate then transforms into a [Ni(II)-butenyl]+ complex (Step 3, Scheme 3a) that rotates (Step 4, Scheme 3a) to form an agostically bound [Ni(II)-butadiene-H]+ complex. Adsorption of a third ethene molecule (Step 5, Scheme 3a) followed by βhydride transfer eliminates 1,3-butadiene (Steps 6 and 7, Scheme 3a), forming a non-agostic [Ni(II)-hydride-ethene]+ intermediate. This intermediate readily transforms into an agostic [Ni(II)-ethyl]+ species (Step 8, Scheme 3a), which then undergoes coordination to a fourth ethene to form a [Ni(II)ethyl-ethene]+ species (Step 9, Scheme 3a) that is the presumptive coordination-insertion active site. The calculated free energy difference between the non-agostic [Ni(II)-hydrideethene]+ and the agostic [Ni(II)-ethyl]+ species is only 2 kJ mol-1, suggesting facile insertion of ethene into [Ni(II)-hydride]+ to form the coordination-insertion active site.38 This would be consistent with experimental ethene oligomerization data on Ni-Beta that showed the induction period was eliminated upon co-feeding H₂.³³ Although this DFT-calculated pathway suggests formation of 1,3-butadiene and additional surface Brønsted acid (H+) sites during catalyst activation, gaseous 1,3-butadiene or new OH groups were not detected experimentally in the operando IR study.⁵⁴ It is possible, however, that 1,3-butadiene remains adsorbed on any H⁺ sites that may be generated in situ; support for this proposal is evident from operando IR via peaks for CH₂ and CH₃ groups appearing at 225 K and prior to the first detection of butene products in the gas-phase (at 240 K).54 Further evidence for the formation of additional H⁺ sites during the activation period would strengthen this mechanistic proposal (Scheme 3).

In addition to Ni(II) as the precursor to the active intermediates, [Ni(II)-OH] $^+$ is also proposed to be a candidate precursor structure. Experimental evidence for this site proposal is the observation that ethene dimerization rates (per g_{cat} , 243 K, 15 bar C_2H_4) increased linearly with Ni content, until a value of 1 Ni exchanged per H $^+$ site initially present on MCM-41 supports, and were independent of Ni content thereafter; 56 more recent reports demonstrated this for dimerization rates of ethene, propene and butene reactants. 57 The formation of active intermediates from [Ni(II)-OH] $^+$ has been calculated by DFT 38 and the reaction pathway shown in Scheme 3b. This pathway involves coordination and migratory insertion of

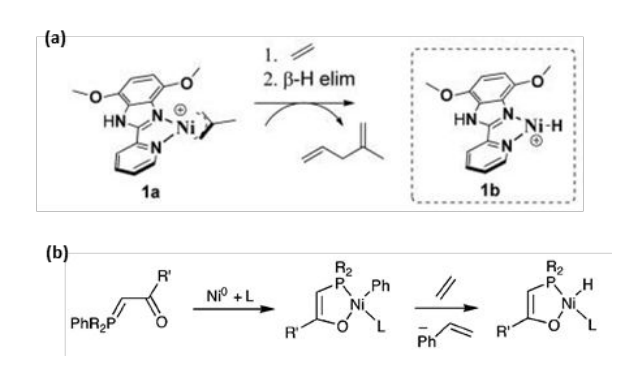
ethene into the Ni-OH bond to form a [Ni(II)-ethene-OH]⁺ species (Steps 1 and 2, Scheme 3b), which rotates to form an agostically bound [Ni(II)-ethenol-H]⁺ species (Step 3, Scheme 3b). This is followed by coordination of second ethene (Step 4, Scheme 3b) and β -hydride transfer (Step 5, Scheme 3b) to eliminate ethenol (Step 6, Scheme 3b) and form the non-agostic [Ni(II)-hydride-ethene]⁺. This then undergoes ethene insertion into the hydride and coordination with a third ethene, as described for the pathway for Ni²⁺ precursor structures, to form the coordination-insertion active site ([Ni(II)-ethyl-ethene]⁺) (Step 7, Scheme 3b). The eliminated ethenol molecule is also proposed to undergo tautomerization to form ethanal (Step 6', Scheme 3b). An alternative pathway for the formation of coordination-insertion active sites from [Ni(II)-OH]⁺ was also

hypothesized by the same set of authors³⁸ as shown in Scheme 3c⁵⁸, following the experimental evidence for the [Ni(II)-ethenyI]⁺ species.⁵⁴ This pathway involves the same initial step of ethene coordination and migratory insertion into the Ni-OH bond (Steps 1, 2, 3 of Scheme 3c = Steps 1, 2 and 3 of Scheme 3b), as described for the ethenol elimination pathway. This species, however, then coordinates to a second ethene molecule (Step 4, Scheme 3c) and eliminates a water molecule to form a [Ni(II)-ethenyl-ethene]⁺ intermediate similar to the case of starting with Ni²⁺ (Step 1, Scheme 3a).⁵⁸ This [Ni(II)-ethenyl-ethene]⁺ intermediate is then proposed to undergo the same elementary steps (Steps 5-10,

Scheme 3 Proposed mechanistic pathways for the formation of coordination-insertion active site starting from (a) an ion-exchanged Ni²⁺ cation (adapted with permission from Henry et al.⁴⁷), (b) a [Ni(II)-OH]⁺ site involving ethanal formation (adapted from Brogaard et al.³⁸), and (c) a [Ni(II)-OH]⁺ site involving 1,3-butadiene formation (adapted from Brogaard et al.)⁵⁸.

Scheme 3c) as described in Scheme 3a (Steps 2-9, Scheme 3a) to form the coordination-insertion active sites. DFT or experimental evidence supporting the proposed [Ni(II)-OH]⁺ activation pathway involving the elimination of water (Scheme 3c), however, is lacking, motivating future research to provide further support for or to falsify this hypothesis. In contrast to the proposed Ni²⁺ activation pathway, the proposed pathways for [Ni(II)-OH]⁺ do not involve the formation of surface Brønsted acid (H⁺) sites. The formation of ethenol (or ethanal) or 1,3-butadiene during the activation of materials containing [Ni(II)-OH]⁺ structures is also not reported experimentally.

The activation of Ni-based oligomerization catalysts involves a stoichiometric (and not catalytic)³⁸ conversion of Ni²⁺ sites into the coordination-insertion active sites, which is followed by catalytic cycles for alkene oligomerization. The formation of coordination-insertion active sites in the absence of external activators for these inorganic materials is similar to certain homogeneous molecular Ni catalysts, such as the methallyl Ni and the Shell Higher Olefins Process (SHOP) type catalyst systems, examples of which are shown in Scheme 4a and 4b, respectively. The methallyl Ni complex essentially serves as a 'pre-catalyst', eliminating the methallyl ligand from the Ni cation in the presence of ethene to form the Ni-hydride species that initiates coordination-insertion cycles (Scheme 4a).37 Similarly, in the case of the SHOP-type catalyst, the 'precatalyst' is first formed by oxidative addition of a keto-stabilized phosphorous ylide to a Ni(0) complex, which upon addition of ethene eliminates the styrene ligand to form the active complex containing the Ni-hydride (Scheme 4b). 11, 36 The Ni2+ cations and [Ni(II)-OH]+ species on porous aluminosilicates can thus be considered to behave as precursors that form the corresponding 'pre-catalyst' intermediates in situ, which then eliminate ligands such as 1,3-butadiene to generate [Ni(II)-H]+ intermediates that serve as coordination-insertion active sites.

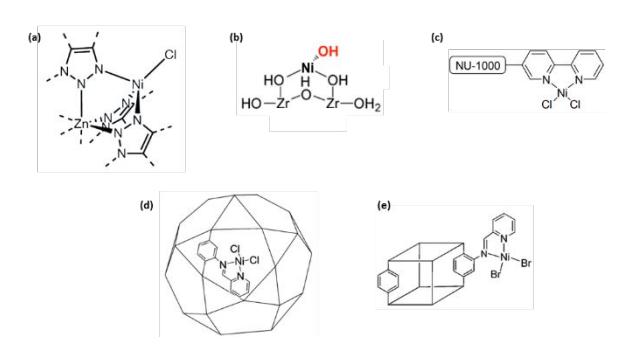


Scheme 4 Formation of active Ni-hydride complex from (a) methallyl Ni compound (adapted with permission from Escobar et al. 37), and (b) a SHOP-type (Shell Higher Olefins Process) catalyst (adapted with permission from Kuhn et al. 59).

2.2 Mechanisms of Ni activation on MOF supports

Alkene oligomerization is catalyzed by Ni sites supported on metal organic frameworks (MOFs) such as MFU-4l, 52 , 60 NU-

1000,⁶¹ and (Fe)MIL-101,⁶² among others, in the presence of external activators or co-catalysts. The requirement of co-catalysts to initiate alkene oligomerization cycles is perhaps unsurprising for MOF supports, because these materials are synthesized to contain Ni sites resembling the homogeneous Ni catalysts that initiate oligomerization cycles only in the presence of such co-catalysts. Ni-containing MOFs are generally considered to catalyze alkene oligomerization via the coordination-insertion mechanism, by analogy to their homogeneous Ni counterparts. Specific experimental and computational evidence for coordination-insertion mechanism has been reported in the case of Ni-MFU-4^[53] and Ni-NU-1000.⁶³



Scheme 5 Structure of Ni(II) precursor sites within the metal organic frameworks: (a) Ni-MFU-4I, (b) Ni-AIM-NU-1000, (c) Ni-NU-1000-bpy, (d) Ni@(Fe)MIL-101, and (e) Ni-MixMOF. Adapted with permission from (a) Comito et al.⁵⁰, (b) Bernales et al.⁵³, (c) Madrahimov et al.⁵¹, (d) Canivet et al.⁵² and (e) Liu et al.⁶⁴

Ni-MOFs differ in their structural chemistry and in their requirement for co-catalysts to initiate the coordinationinsertion cycles. Scheme 5a-e shows the Ni(II) site structures within MOFs that are often present as a mono-anionic or dianionic species, with the anions comprising halides (Cl-, Br-) or hydroxides (OH-) and with the Ni center covalently bonded to the organic framework. In the case of the mono-anionic Ni(II) species (e.g. Ni-MFU-4I), the Ni(II) center is partially chargecompensated by the negatively charged (-1) framework, while in the case of a di-anionic Ni(II) species (e.g. Ni-NU-1000-bpy), the framework is charge neutral. These species initiate alkene oligomerization cycles after adding organoaluminum compounds that serve as co-catalysts, such methylaluminoxane ([Al(CH₃)O]_n, MAO), diethylaluminum chloride (Et₂AlCl) or triethylaluminium (Et₃Al), to the reaction mixture containing a solvent, the alkene monomer and the Ni-MOF. In the case of Ni-MFU-4I, the mono-chloride Ni(II) species (Scheme 5a) is efficiently transformed into its active form using MAO, while the use of Et₂AlCl as an activator led to a ~4-fold decrease in the oligomerization rate under identical reaction conditions.⁵² For other Ni-MOFs, such as Ni-AIM-NU-1000,⁶⁵ Ni-NU-1000-bpy,⁶¹ Ni-MixMOF,⁶⁴ and Ni@Fe(MIL)-101,⁶² MAO was not used as an activator while only Et₂AlCl has been used. In general, external activators present in large stoichiometric excess (50-5000 molar equivalents per Ni) are required to initiate alkene oligomerization on Ni-MOFs,52,61,62,64 in part because these organoaluminum compounds are present as

Mini review

(a)
$$\begin{array}{c} L \\ L \\ Ni - A \end{array} + \underbrace{(Al(CH_3)O)_{x+1}}_{C} \underbrace{\begin{array}{c} L \\ L \\ \end{array}}_{L} Ni \underbrace{\begin{array}{c} R' \\ \end{array}}_{R'} + \underbrace{\begin{array}{c} (Al(CH_3)O)_{x} \\ \underline{or} \end{array} (Et_2AlCl)_{x}}_{R'} \end{array}$$

$$\begin{array}{c}
L \\
Ni \\
A
\end{array} + \underbrace{(AI(CH_3)O)_{x+1}}_{A} + \underbrace{or}_{(Et_2AICI)_{x+1}} \\
- \underbrace{or}_{A} + \underbrace{or}_{A} (Et_2AICI)_{x+1}
\end{array}$$

$$\begin{array}{c}
L \\
A \\
Or (Et_2AICI)_{x}
\end{array}$$

$$\begin{array}{c}
C \\
A \\
Or (Et_2AICI)_{x}
\end{array}$$

$$\begin{array}{c}
C \\
A \\
Or (Et_2AICI)_{x}
\end{array}$$

$$\begin{array}{c}
C \\
A \\
Or (Et_2AICI)_{x}
\end{array}$$

Scheme 6 Generalized reaction pathway for the formation of coordination-insertion active sites using MAO ($[Al(CH_3)O]_{x+1}$) or Et_2AlCl activators in presence of ethene from (a) Mono-anionic Ni(II), and (b) Di-anionic Ni(II) precursor species in MOFs. L = Linking group within the Ni(II) species; A = Halide (X^2), Hydroxyl ion (OH'); R' = H (for MAO), CH₃ (for Et_2AlCl); x represents an oligomeric structure of MAO or Et_2AlCl molecular units.

oligomeric or cage-like structures that contain only a small fraction of terminal alkyl-aluminum groups, ⁶⁶⁻⁶⁸ and because these larger structures are thought to encounter diffusional constraints when attempting to access Ni sites within MOF supports. ⁵³ Moreover, during the activation process using these alkyl-aluminum compounds, the Ni sites within the MOF structures retain an oxidation state of +2. ⁶⁰

The mechanism to form the coordination-insertion active sites in Ni-MOFs is not reported explicitly, but is implied to resemble that of their homogeneous Ni analogs. Scheme 6a and 6b show a generalized reaction pathway based on the activation of Ziegler-Natta catalyst systems^{67, 69, 70} to form coordinationinsertion active sites from Ni(II) mono-anionic and di-anionic precursor species, respectively. In the case of a Ni(II) monoanionic species (Scheme 6a), the anion (A-) is exchanged with one alkyl group from the activator, and coordination with the reactant ethene forms the active site (Ni-alkyl-ethene). In the case of a Ni(II) di-anionic species (Scheme 6b), the first step involves a similar exchange of an anion (A-) with one alkyl group from the activator, and the second step involves the activator abstracting the second anion (A-) to generate a vacancy for ethene coordination to form the active site. The active cationic Ni(II) species, however, exists as an ion-pair with the anionic activator species, which is stabilized by the organic solvent as in the case for Ziegler-Natta catalysts.⁶⁹⁻⁷¹ Although the formation of Ni(II) active sites in MOFs can be adapted from that on homogeneous Ziegler-Natta catalysts, a definitive mechanistic pathway for the activation of these homogeneous catalysts itself is uncertain, mainly because these activators are present in different structural forms (chains, rings, sheets and cage structures) that exhibit distinct activation efficiencies and are present in dynamic equilibria. 66, 68

Ni-MOFs such as Ni-MOF-74 $(Ni_2(dobdc))$, 72 $Ni_2(dobpdc)$ and Ni-UiO-67-bpy 73 are demonstrated to catalyze alkene chain growth reactions in the absence of alkylaluminum co-catalysts. Propene oligomerization (453 K, 5 bar C_3H_6) on Ni-MOF-74 and Ni₂(dobpdc) in a continuous fixed-bed reactor after pretreatment in He (453 K, overnight) showed an induction period during initial reaction times. The induction period was hypothesized to reflect the coordination of propene to a Ni²⁺

site and displacement of at least one Ni-O ligand interaction to form the active [Ni(II)-alkyl]+ site, however, other mechanistic possibilities for activation were not excluded.⁷² Similarly, ethene oligomerization (523 K, 26 bar C₂H₄, 4 bar N₂) on Ni-UiO-67-bpy in a continuous fixed-bed reactor after an oxidative pretreatment (573 K, 6h, 10% O₂) showed an induction period during initial reaction times. 73 The Ni-UiO-67 sample with bpdc (biphenyl-4,4'-dicarboxylic acid) linkers but not bpy (2,2bipyridine-5,5-dicarboxylate) linkers was inactive for ethene dimerization, however, samples with varying bpy linker concentrations and similar Ni/bpy ratios showed nearly identical induction periods, implicating a role of the bpy linkers in activating Ni(acetate) precursor structures.73 Induction periods on Ni-UiO-67 samples shortened with increasing Ni loading for the same concentration of bpy linkers in the MOF, suggesting that a higher density of Ni acetate precursors favor the formation of the Ni active site or of multimeric Ni active sites.⁷³ Although these studies provide preliminary hypotheses for the activation of Ni-MOFs in absence of co-catalysts, opportunities exist to obtain further mechanistic evidence.

In summary, the requirement of an activator for porous Nibased alkene oligomerization catalysts is determined by the structure of the precursor Ni(II) sites. In the case of ionexchanged Ni²⁺ and [Ni(II)OH]⁺ sites within inorganic microporous and mesoporous materials, Ni(II) centers contain vacant coordination sites, because organic ligands and anions are absent unlike in Ni-MOFs. As a result, these Ni(II) cations more readily coordinate alkenes and activate their C-H bonds in absence of an activator to form the reactive intermediates (Niethenyl, Ni-hydride). In contrast, Ni(II) cations in MOFs contain charge-compensating anions in the form of halides or hydroxides that prevent alkene coordination and direct formation of Ni-C bonds in the absence of the co-catalysts or activators. Once an activator is added, however, chargecompensating anions are abstracted and Ni-alkyl species are formed, allowing for alkene coordination to the Ni(II) center and insertion into Ni-alkyl bonds to initiate coordination-insertion cycles. Thus, the requirement of an external activator is dictated by the unavailability of vacant coordination positions in Ni(II)

precursor structures that are required to activate alkene C-H bonds and generate Ni-alkyl species.

3. Catalyst deactivation during alkene oligomerization

3.1 Mechanisms of Ni deactivation on microporous and mesoporous inorganic supports

Alkene chain growth reactions on Ni-containing zeolites (FAU, $^{49, 74, 75}$ Beta, $^{33, 47}$ MFI, 47 MWW 76 , AFI 58) and mesoporous materials (MCM-41,77 MCM-36,76 MCM-48,77 SBA-1577,78) are often accompanied by catalyst deactivation. Although one study reported no deactivation during ethene oligomerization (393 K, 26 bar C₂H₄) on a nanocrystalline (~25 nm) Ni-Beta sample (Si/Al = 12, 2 wt.% Ni), another study showed that a similar nanocrystalline (<50 nm) Ni-Beta sample (Si/Al = 17.4, 2.1 wt.% Ni) did deactivate under similar conditions (393 K, 25.1 bar C₂H₄), consistent with other studies involving Ni-zeolite catalysts of varying compositions tested under a range of oligomerization reaction conditions. $^{\rm 33,\ 47,\ 49,\ 58,\ 74-77,\ 79}$ We note that catalyst deactivation will be observed given pathways to reduce Ni cations to their metallic state, as Ni(0) is not known to catalyze alkene chain growth reactions.^{43, 80} The deactivation of these materials is generally correlated with the formation of heavier oligomers; for example, Ni-MCM-41 samples that formed larger fractions of high molecular weight oligomers from ethene oligomerization also showed faster deactivation rates.81 Furthermore, in the case of Ni-MCM-4181 and Ni-MCM-36⁷⁶ samples, higher H⁺/Ni site ratios and reaction temperatures favored forming higher molecular weight oligomers, and led to faster deactivation of these samples. Therefore, higher molecular weight products are purported to more strongly adsorb at active sites and block porous voids of the support, both of which would lead to deactivation.2

In cases where deactivation has been observed, the products adsorbed on the catalyst surface during deactivation have been studied by operando IR, wherein air-pretreated H-MFI and Ni-H-MFI samples were exposed to short pulses of dilute ethene (0.4 bar C₂H₄) followed by inert flush at different temperatures (423, 473, 573 and 673 K), while monitoring the effluent using a mass selective detector (MSD). In the case of H-MFI, unsaturated carbenium ions (1505 and 1537 cm⁻¹) and small amounts of polycondensed aromatics (1597 cm⁻¹) were predominantly observed at temperatures that led to rapid deactivation; thus, their formation was proposed to deactivate the H⁺ sites. Similarly, in the case of Ni-H-MFI, polycondensed aromatics (1597 cm⁻¹) and polyconjugated aliphatics (1635 cm⁻¹ 1) were predominantly formed at temperatures leading to rapid deactivation; thus, their formation was proposed to deactivate Ni-H-MFI. In case of both H-MFI and Ni-H-MFI, however, v(C-H)stretching vibrations of adsorbed alkenes (>3000 cm⁻¹) were not observed under every temperature studied; therefore, deactivation was not proposed to be caused by heavier oligomers.⁷⁹ In contrast, deactivated Ni-H-Beta samples after ethene oligomerization (423 K) at high pressures (26 bar C₂H₄) were characterized ex situ by extracting the retained hydrocarbons using dichloromethane and dissolving the catalytic solids in HF, which showed the presence of surface bound C₁₀-C₁₄ alkenes but no aromatic compounds.⁴⁷ The differences in species adsorbed on Ni-H-MFI and Ni-H-Beta may reflect the different reaction conditions (temperature, ethene pressures) during catalyst deactivation, the different Ni and H⁺ site contents on the Ni-H-MFI (Si/AI = 59, 2 wt.% Ni) and Ni-H-Beta (Si/Al = 17.4, 2.1 wt.% Ni) samples, as well as differences in their pore topology. In summary, the deactivation of Nicontaining zeolites during alkene oligomerization is proposed to be caused by strongly adsorbed hydrocarbons, which have been proposed variously to be heavier oligomers, polyconjugated aliphatic compounds or polycondensed aromatics formed by Htransfer and cyclization reactions similar to those that occur during methanol-to-hydrocarbon catalysis.82, 83 Experimental studies have explored aluminosilicate supports containing both Ni and H⁺ sites, but the deactivation of Ni sites alone in the absence of residual H⁺ sites has yet to be studied.

Deactivation during alkene oligomerization has also been correlated to the pore structure of the support, as Ni-based microporous zeolites are generally observed to deactivate more rapidly than mesoporous materials.2 For example, under identical reaction conditions (batch, 423 K, 40 bar C2H4), a microporous Ni-MCM-22 (10-MR, 0.55 × 0.4 nm diam.) sample deactivated more rapidly than a mesoporous Ni-MCM-36 (inner-free dimensions of $0.71 \times 0.71 \times 1.82$ nm) sample.⁷⁶ This was attributed to pore blocking by heavier oligomers, based on a higher thermogravimetric (TGA) weight loss measured for the deactivated Ni-MCM-22 sample than the deactivated Ni-MCM-36 sample. 76 Similarly, a series of Ni-containing dealuminated Y zeolites that were deactivated under identical reaction conditions showed lower masses of carbonaceous deposits (by TGA) as the fraction of mesoporous voids increased, interpreted to promote diffusion of heavier molecular weight species.84

Although differences in the deactivation behavior observed between Ni-based mesoporous and microporous materials have been attributed to differences in their pore structures, their observed deactivation transients also reveal key mechanistic distinctions. For example, during propene oligomerization under the same reaction conditions (453 K, 1 bar C_3H_6), mesoporous Ni-Na-MCM-41⁷⁷ and microporous Ni-Na-X⁴⁹ catalysts exhibit transient deactivation of rates that decay with either an exponential or hyperbolic dependence, respectively. 49,77 Exponential deactivation was attributed to the formation of oligomers larger than dimers that do not desorb under the reaction conditions tested and thus block active sites, 77 while hyperbolic deactivation was attributed to the involvement of two Ni sites in each deactivation event. 49

Hyperbolic deactivation behavior has been proposed to reflect interaction between two proximal alkene-bound Ni²⁺ intermediates that form a bridged alkene complex, as shown in Scheme 7.⁴⁹ The formation of such a complex was supported by the observation that no other gas-phase products or surface intermediates (observed by IR) other than oligomers were formed during the deactivation period.⁴⁹ The involvement of two Ni sites in a single deactivation event is supported by a

deactivation rate model that shows a second-order dependence on the concentration of alkene-bound Ni²⁺ intermediates. This second-order model describes measured deactivation transients for Ni-Na-X samples after considering the fraction of active Ni sites and the initial distribution of Ni²⁺ cations between the sodalite cages and the hexagonal prisms of FAU. Further, the extent of deactivation, taken as the difference between the maximum propene consumption rate and that measured after 1.5 hours had elapsed from the maximum measured rate, was found to increase with Ni content on Ni-Na-X samples. Additionally, the second-order deactivation model sufficiently captured the transient experimental data irrespective of the Ni loadings (0.16-5.90 wt.%) on these samples.

Based on these results, this experimental study⁴⁹ proposes that the deactivation rate increases with Ni content, but the mechanism of deactivation is not a function of the proximity between Ni sites, suggesting that alkene-bound Ni²⁺ intermediates might be mobile within the supercages of zeolite X under reaction conditions.⁴⁹ The concept of alkene-conferred mobility to Ni²⁺ cations has also been proposed using DFT-based molecular dynamics (DFT-MD) simulations⁵⁸ that show mobile Ni(II) complexes to be involved in the coordination-insertion cycle for alkene oligomerization (Ni-AFI, 393 K, 25 bar C_2H_4), and experiments under corresponding reaction conditions (Ni-AFI, 393 K, 4–25 bar C_2H_4) exhibit a hyperbolic deactivation transient similar to Ni-Na-X.⁵⁸

$$\begin{array}{c|c}
C_{n} & R & C_{m} \\
\hline
 & C_{m} & N_{1} & N_{2} & N_{3}
\end{array}$$

$$\begin{array}{c|c}
C_{n} & C_{m} &$$

Scheme 7 Proposed structure of a deactivated Ni species with a shared bridging alkene between two Ni cations. Lengths of alkene chains on the Ni cations are indicated by m and n (adapted with permission from Mlinar et al.⁴⁹)

Although the deactivation mechanism remained unchanged on Ni-Na-X samples of varying Ni density, 49 a significantly lower Ni density in mesoporous supports is reported to lead to an exponential rather than a hyperbolic deactivation transient. Table 1 summarizes the type of deactivation transients during alkene oligomerization as a function of the Ni density within mesoporous and microporous materials. Ni-containing microporous zeolites with a higher Ni density than mesoporous materials (MCM-41, SBA-15) show a hyperbolic deactivation transient, implying that more than one Ni site participates in each deactivation event. In contrast, Ni-containing mesoporous materials (MCM-41, SBA-15) with lower Ni density show an exponential deactivation transient, implying a single-site deactivation mechanism. In general, the deactivation mechanisms of Ni-containing porous materials during alkene oligomerization are observed to change with Ni density, but the underlying mechanistic details are incompletely understood.

Reaction conditions for ethene oligomerization on Ni-MCM-41 that favor the formation of an intrapore condensed liquid phase are shown to be more selective towards light oligomers (dimers) than heavy molecular weight products and also

suppress catalyst deactivation.⁵⁶ Ni-MCM-41 samples exhibit exponential deactivation under the conditions of gas-phase ethene oligomerization at 243 (1 bar) and 253 K (1.5 bar).56 The first-order deactivation constants (243 K and 253 K) decrease with increase in ethene pressure, and no deactivation is detected at ethene pressures that correspond to the filling of MCM-41 pores with liquid ethene (as determined from N₂ adsorption isotherms (77 K) to approximate ethene adsorption and pore filling).⁵⁶ The selectivities toward C₄ alkene products and 1-butene also increase in the presence of intrapore liquid ethene, suggesting the preferential solvation of the later transition states that mediate desorption events over the earlier transition states that mediate the growth and isomerization of adsorbed 1-butene. Thus, the absence of deactivation is attributed to the presence of intrapore liquids that favor desorption of 1-butene, suppressing subsequent isomerization and chain growth reactions that lead to the formation of stranded oligomers to deactivate Ni sites.⁵⁶ This observation resembles that of 1-butene oligomerization on H-FER, wherein low temperature (423 K) and near-supercritical conditions inhibit catalyst deactivation, attributed to the solvent-like properties of butene under these conditions that enable extraction of heavy oligomer products from the catalyst pores.85

3.2 Mechanisms of Ni deactivation on MOF supports

Ni-containing MOFs deactivate rapidly during alkene oligomerization and often require complex regeneration procedures to avoid structural degradation.3 Many catalytic studies of Ni-MOFs have been carried out in batch or semi-batch reactors, while fewer have been carried out in continuous flow reactor configurations. Batch reactor studies commonly report the turnover frequency and oligomer yield based on the cumulative amount of products formed at the end of a reaction experiment, and deactivation models are often not developed or reported, preventing quantitative assessments of catalyst stability.86 Deactivation has generally been probed by characterizing spent samples and testing them again in subsequent batch reaction experiments. MOFs also differ in structural coordination and chemical composition, and thus cannot be classified based on their pore size as can inorganic oxide molecular sieve supports whose frameworks are comprised of corner-sharing tetrahedra. As a result, many different proposals for the deactivation of Ni-MOFs during alkene oligomerization have been reported.

The deactivation of Ni@(Ti)MIL-125,⁸⁷ Ni@(Fe)MIL-101⁶² and Ni-UiO-67-bpy⁷³ during ethene oligomerization has been purported to be caused by formation of oligomeric or polymeric products that do not desorb under reaction conditions. The deactivation of Ni@(Ti)MIL-125⁸⁷ (323 K, 10 bar, cyclohexane, 0.5 h, MAO Al/Ni = 800) and Ni@(Fe)MIL-101⁶² (283 K, 15 bar, heptane, 1 h, Et₂AlCl Al/Ni = 70) was assessed by recovering spent samples after semi-batch experiments of ethene oligomerization, washing with anhydrous ethanol, drying and re-using them for ethene oligomerization by activating with excess co-catalyst. Measured oligomer yields decreased slightly

Table 1 Effect of Ni density and reaction conditions on the type of deactivation transient for Ni-based porous aluminosilicate materials

Material Ni/Al	Ni spatial density	Feed	Temp.	Pressure	Deactivation	Ref.	
	[atoms nm ⁻³] ^a	Alkene	[K]	[bar]	Transient		
Ni-Li-Beta	0.26	0.82	Ethene	453	0-0.01	Hyperbolic	33
Ni-H-Beta	0.83	1.20	Ethene	393	25.1	Hyperbolic	47
Ni-Na-X	0.28	3.52	Propene	453	1-5	Hyperbolic	49
Ni-H-AFI	0.34	0.26	Ethene	423	26	Hyperbolic	58
Ni-H-SBA-15	n/a	0.42 ^b	Ethene	423	30	Exponential	78
Ni-Na-MCM-41	0.14-0.52	0.05-0.18 ^b	Propene	453	1	Exponential	77
Ni-H-MCM-41 ^c	5.0	1.11 ^c	Ethene	448	15	Exponential	56

 $^{^{}a}$ Calculated as (Ni atoms per g_{cat})/(Micropore volume per g_{cat}) using reported Ni wt. % loading and adsorption data

during the second catalytic run for both Ni@(Fe)MIL-10162 and Ni@(Ti)MIL-12587, while subsequent catalytic runs showed significant decrease in oligomer yield for Ni@(Ti)MIL-125,87 which was proposed to be caused by adsorbed residual oligomers and MAO at the active sites.87 In the case of Ni-UiO-67-bpy,⁷³ deactivation was evident from the decrease in butene formation rate with reaction time during continuous gas phase ethene oligomerization (523 K, 26 bar C₂H₄, 4 bar N₂, no cocatalyst) and was investigated by TGA, N2 adsorption, XRD and IR characterization of the spent samples. As compared to the fresh sample, the spent sample had higher weight loss (by 15%) via combustion during TGA, and a lower specific surface area by N₂ adsorption despite no structural degradation observable by XRD. IR characterization concluded that the residual hydrocarbons on the spent sample consisted of oligomers smaller than octenes, by comparing the observed relative intensities of IR peaks for -CH2 and -CH3 groups with those of 1octene. Based on these results, the deactivation of Ni-UiO-67bpy was proposed to be caused by carbonaceous deposits consisting of oligomers longer than butene, but smaller than octene. Although XRD did not show evidence for the formation of crystalline or amorphous polyethylene, ethene conversion did not exceed 6% on the Ni-UiO-67-bpy sample studied; the effect of higher conversion on the chain lengths of oligomers that comprise the carbonaceous deposits remains unknown. On the other hand, the deactivation of Ni-NU-1000 is proposed to reflect formation of polymeric products. During gas-phase continuous ethene oligomerization, Ni-AIM-NU-1000⁶⁵ (318 K, 0.2 bar ethene, Et₂AlCl, Al/Ni = 70) prepared by atomic-layer deposition (ALD) and Ni-NU-1000-bpy⁶¹ (297 K, 2 bar, Et₂AlCl, Al/Ni = 70) deactivated with time, attributed to the formation of polymeric products observed by SEM of spent samples.^{61, 65}

Deactivation mechanisms for Ni-MOFs are also proposed that do not involve formation of heavy oligomeric or polymeric products, often to rationalize situations in which such species are not detected or are formed in minority amounts. For example, ethene oligomerization on Ni-MFU-4I⁵² and Ni-CFA-1⁸⁸ showed only traces of polyethylene in the product⁵² and on the

spent samples as determined by XRD. The deactivation of Ni-MFU-4I (10 wt.% Ni) during ethene oligomerization (50 bar, toluene, MAO, 1 h batch) at ambient temperature was assessed by removing the products from the batch reactor by distillation and re-pressurizing the reactor with ethene.52 After repeating this process 8 times, an 18% decrease was observed in the mass of isolated butene products relative to that on the fresh sample, indicating deactivation occurred.⁵² The underlying mechanistic details were investigated by X-ray absorption spectroscopy of the fresh and spent Ni-MFU-4l samples subjected to ethene oligomerization (50 bar, toluene, MMAO-12, 24 h batch) at ambient temperature.88 Ni K-edge data for the spent sample showed that the absorption edge shifts towards lower energies approaching that of Ni foil, and EXAFS analysis showed presence of Ni-Ni scattering, suggesting partial reduction of Ni²⁺ cations to metallic Ni. On the other hand, EXAFS analysis of Zn K-edge data for the spent Ni-MFU-4l sample showed no features for Zn-Zn scattering, indicating that framework Zn2+ sites did not reduce to metallic Zn. Furthermore, a control experiment involving treatment of Ni-MFU-4l with the co-catalyst (AlMe₃, 14 h) showed the presence of supra-stoichiometric amounts of Al on the spent sample, while the same experiment on the MFU-4l support (without Ni) led to only trace amounts of Al on the spent MFU-4l sample. These combined findings led to the deactivation mechanism of Ni-MFU-4l proposed in Scheme 8, which involves reductive demetallation of Ni²⁺ to form metallic Ni nanoparticles along with incorporation of alkylaluminum into the vacant secondary building sites of MFU-4l generated upon removal of Ni²⁺ cations.⁸⁸ Additionally, AlMe₃ treatment of Tp^{Mes}NiCl (Tp^{Mes-} = tris(3-mesityl-1-pyrazolyl)borate), the homogeneous analog for the Ni active site in Ni-MFU-4I, also showed formation of metallic Ni, supporting the reductive demetallation mechanism in Ni-MFU-4l deactivation, although pure aluminum complexes were not isolated and analyzed.88 The Ni-CFA-1 MOF that contains homologous node structures as Ni-MFU-4l showed a loss of crystallinity (based on XRD) with increasing batch reaction time, consistent with the formation of alkylaluminum species (Scheme 8) that lose crystallinity on

^bCalculated as (Ni atoms per g_{cat})/(Mesopore volume per g_{cat}) using reported Ni wt. % loading and adsorption data

 $^{^{}c}$ Calculated as [(Ni atoms per nm $^{-2}$) x (Specific surface area, nm $^{-2}$ per g_{cat})] / (Mesopore volume per g_{cat}) using reported Ni density (Ni atoms nm $^{-2}$) and adsorption data n/a – not available from reported information

Mini review

exposure to air, but not an air-free environment. Thus, Ni-CFA-1 was also proposed to deactivate by reductive demetallation, although X-ray absorption characterization analogous to Ni-MFU-4l was not reported.⁸⁸

Scheme 8 Proposed mechanism for deactivation of Ni-MFU-4l via reductive demetallation (reproduced with permission from Metzger et al.⁸⁸)

In summary, the deactivation of Ni-containing MOFs has been attributed to either adsorbed oligomers and activators at the active site structures, formation of polymeric deposits, or reductive demetallation. Among these deactivation routes, reductive demetallation of Ni active site structures has been studied mechanistically in the case of Ni-MFU-4I, while the mechanistic details of deactivation for other materials remain to be determined. Generalizing the deactivation mechanism and routes among Ni-MOF materials does not appear possible because of the distinct structure and composition of their linkers and nodes.

4. Kinetics of alkene chain growth reactions on Ni-based catalysts

4.1 Kinetics on Ni-based microporous and mesoporous inorganic supports

Alkene chain growth reaction rates (393–453 K) have been measured at Ni sites on aluminosilicate supports more so than on other supports. The measurement of rates at Ni sites of these materials, however, is often complicated by contributions from side reactions such as cracking, hydride transfer and aromatization of long chain (>C₅) olefin products on residual H⁺ sites, ⁸⁹⁻⁹¹ and by rapid catalyst deactivation. Further, Ni precursor sites on these materials are proposed to exist in various forms including exchanged Ni²⁺, [NiOH]^{+,56} Ni²⁺ grafted at acidic silanol groups^{54,92} and undercoordinated Ni²⁺ sites at NiO nanoparticle surfaces. ⁹² Reaction rates on these various Ni precursor sites have been determined at different reaction conditions and with different methodologies for kinetic measurements and data analysis, leading to different interpretations of alkene chain growth kinetics.

The kinetic parameters determined for alkene chain growth reactions (393–453 K) on exchanged Ni²⁺ cations in zeolites are summarized in Table 2, and indicate the various reaction orders measured for alkene chain growth reactions. These kinetic measurements on exchanged Ni²⁺ cations in zeolites have considered pseudo-steady-state rates (except for Ni-LTA) obtained after initial rapid deactivation, which are often

significantly lower than those measured at initial reaction times, and are discussed in detail below. Also, the measured rates of alkene dimerization and trimerization reflect the net formation rate of dimer and trimer species, which are consumed in subsequent reactions of the oligomerization network and that form intermediates leading to catalyst deactivation. Thus, such measurements would not reflect intrinsic turnover rates of alkene chain growth reactions, which are determined by forward reaction rates normalized by the number of Ni active sites under reaction conditions.

Propene oligomerization rates (453 K, 1-5 bar) on Ni-X (i.e., Ni-FAU) zeolites have been measured on a low Ni content (0.6 wt.% Ni) sample following air treatment (773 K, 3 h) once pseudo-steady-state was achieved after partial deactivation.⁴⁹ This Ni-X sample was first contacted with propene (5 bar) at 493 K to shorten the induction period by promoting the migration of Ni²⁺ cations to FAU supercages and to accelerate the deactivation transient,49 after which pseudo-steady-state dimer and trimer formation rates were found to show a first-order and second-order dependence on propene pressure, respectively (Table 2). Dimer and trimer formation rates extrapolated to give finite values at zero propene pressure, attributed to oligomerization on alkene-saturated H+ sites at rates assumed to be zero-order in propene pressure.⁴⁹ The pseudo-steadystate propene consumption rate (453 K, 5 bar) was ~63% lower than the maximum rate measured at these conditions.⁴⁹

Ethene dimerization and oligomerization rates (393 K) have also been measured during transient deactivation on Ni-Beta zeolites.⁴⁷ Ni-Beta samples after inert pretreatment (He, 573 K, 16 h) were contacted with ethene (25.1 bar, total pressure of 29 bar) at 393 K, and underwent rapid deactivation during initial reaction times. After 10 h of reaction time, slower deactivation was observed and rates were measured at varying ethene partial pressures (11.6-25.1 bar) with periodic returns to a reference condition (393 K, 25.1 bar C₂H₄).⁴⁷ A deactivation model was formulated to describe transient reaction rates at this reference condition, and used to correct transient rate data to estimate pseudo-steady-state rates (393 K).⁴⁷ The pseudosteady-state ethene consumption and dimer formation rate showed a second-order dependence (Table 2) on ethene pressure (11.6–25.1 bar).47 Pseudo-steady-state rates at the reference condition (393 K, 25.1 bar) were ~45% lower than that measured at initial time on stream, reflecting kinetic data that probed only a fraction of the Ni sites.47

Rates of ethene chain growth reactions on Ni-AFI⁵⁸ have been measured similar to that on Ni-Beta, ⁴⁷ however, using a different reference condition (423 K, 26 bar C₂H₄, 30 bar total). Transient rates for dimer and trimer formation, after correcting for deactivation, were second-order in ethene pressure (Table 2).⁵⁸ Similar to Ni-Beta, the pseudo-steady-state ethene consumption rate was ~33% lower than the rate measured at initial reaction time.⁵⁸ DFT-based molecular dynamics simulations (DFT-MD) were used to model coordination-insertion cycles for ethene oligomerization (393 K) on Ni-AFI, with the equilibrium loading of ethene within the pores estimated by Grand Canonical Monte Carlo simulations at 25 bar.⁵⁸ These simulation results showed reversible mobilization

Table 2 Summary of kinetic parameters for alkene chain growth reactions measured on Ni-based porous aluminosilicate materials

Catalyst	Feed Alkene	Tempera ture [K]	Pressure range [bar]	Chain Growth Reaction	Apparent reaction order	Apparent activation energy [kJ mol ⁻¹]	Ref		
Ni-H-AFI Ethene		423	4-26	Dimerization	2	35 ± 3	58		
	Ethene			Trimerization	2	n.r.			
	Filtra	202	11.6-25.1	Dimerization	2	n.r.	47		
Ni-H-Beta	Ethene	393		Oligomerization	2	n.r.			
Ni-Na-X Propens	_	453	1.25-5	Dimerization	1	45	49		
	Propene			1.25-5	1.25-5	Trimerization	2	n.r.	49
Ni-Ca-LTA 1-Buteno		Dimerization e 433 13.5-41.4 Oligomerization	13.5-41.4			Dimerization	2	73 ± 1	
	1-Butene			Oligomerization	2	73	55		
Ni-Na-MCM-41	Ethene	448	5-25	Dimerization	2	n.r.	56		

n.r. - Not Reported

of Ni²⁺ cations by ethene molecules resulting in a catalytic cycle involving both mobilized and immobilized Ni²⁺ intermediates. Measured pseudo-steady-state rates (408-438 K) showed an apparent activation energy of 35 ± 3 kJ mol⁻¹ (Table 2) at 4 and 26 bar ethene, which was interpreted as reversible mobilization of Ni²⁺ cations occurring across a wide pressure range.⁵⁸

Rates of 1-butene chain growth reactions (433 K) have been measured on Ni-Ca-LTA (6 wt. % Ni), proposed to occur at the pore mouth or extracrystaline surfaces to form linear octenes and methylheptenes as the dominant dimer products.⁵⁵ Kinetic analysis was performed by extrapolating formation rates to initial time to account for deactivation. Initial rates (433 K) showed a second-order dependence on 1-butene pressure (13.5-41.4 bar), with 1-butene adsorption data indicating near saturation coverages of 1-butene.55 Ni-butyl species were proposed to be the active site, with the first two elementary steps involving consecutive adsorption of two gas-phase 1butene molecules, followed by rate-limiting C-C coupling and desorption of the dimer product to regenerate the site. A rate expression was derived by pseudo-steady-state treatments of the Ni intermediates, resulting in a second-order dependence on 1-butene pressure with the Ni-butyl site as the most abundant reaction intermediate (MARI). Apparent activation energies for linear octene (72 kJ mol⁻¹) and methylheptene (76 kJ mol⁻¹) formation (413-453 K) were similar, indicating the involvement of similar transition state structures.55

A microkinetic model for ethene oligomerization on Ni-AFI⁵⁸ provides mechanistic insights regarding the surface coverage of reaction intermediates of the coordination-insertion cycles and its influence on measured reaction kinetics. The role of diffusion was not considered in this study, and the microkinetic model considered a mean-field approximation wherein adsorbates were non-interacting and randomly distributed. The model utilized the free energies of the reaction intermediates at 393 K determined from DFT-MD simulations, and a steady-state solution was obtained at 5% ethene conversion for 25 bar ethene pressure with product pressures that resemble

experimental measurements (423 K, 26 bar C_2H_4 , 30 bar total pressure). Considering the active site to be the [ethene-Ni(II)-ethyl]⁺ species, the microkinetic model showed that the reaction orders for ethene dimerization and trimerization are sensitive to the surface coverage and thus to the free energies of [ethyl-Ni(II)-alkene]⁺ intermediates, and particularly to that of the [ethyl-Ni(II)-butene]⁺ species.

This study⁵⁸ notes that the free energy profile for the coordination-insertion pathway was constructed by combining individual free energy profiles of the elementary steps, and this leads to accumulation of error in the simulated reaction free energies along the pathway. Accordingly, the free energy of [ethyl-Ni(II)-butene]+ species is shown to vary significantly depending on how it was considered to be formed; formation via hydrogen transfer in the [ethene-Ni(II)-butyl] + species led to a lower free energy than formation via ethene desorption from the [ethene-butene-Ni(II)-ethyl]+ species. In the former case, the microkinetic model predicted [ethyl-Ni(II)-butene]+ to be the predominant surface species, leading to dimerization and trimerization reaction orders of ~2.5 and ~1.5, respectively.⁵⁸ In the latter case, the microkinetic model predicted [(ethene)2-Ni(II)-ethyl]* to be the predominant surface species, resulting in dimerization and trimerization reaction orders of ~0.4 and ~(-0.5), respectively.58 Considering an intermediate value for the free energy of [ethyl-Ni(II)-butene]+ species, the microkinetic model predicted comparable surface coverages for both [ethyl-Ni(II)-butene]⁺ and [(ethene)₂-Ni(II)-ethyl]⁺, leading to dimerization and trimerization reaction orders of ~1.2 and ~0.2, respectively.⁵⁸ For the above three cases, a degree of rate control analysis indicated the elementary steps of β -hydride transfer from [ethene-Ni(II)-butyl]⁺ to form [ethyl-Ni(II)butene]+ and the parallel step of [ethene-Ni(II)-butyl]+ coordination with gas-phase ethene to form a mobile [ethene-Ni(II)-butyl]⁺ intermediate to exhibit the highest degree of rate control. Thus, this microkinetic modeling study does not conclusively establish the expected reaction orders for alkene dimerization and trimerization, but reveals their strong dependence on the surface coverages of [ethyl-Ni(II)-alkene][†] intermediates. The study⁵⁸ notes that the uncertainty involved in determining the surface coverages of [ethyl-Ni(II)-alkene][†] intermediates can be overcome by accurately determining the free energies of these species using more advanced methods.

Alkene oligomerization rates (243–453 K) have also been measured on Ni-containing mesoporous aluminosilicate supports (e.g., MCM-41) under steady-state conditions and during transient deactivation. Gas-phase ethene oligomerization has been shown to deactivate Ni-MCM-41, however, reaction conditions that favor the formation of intrapore liquid alkene phases are proposed to inhibit deactivation.⁵⁶ Typically, Ni-MCM-41 samples were first treated in air (823 K, 0.5 h), and then ethene dimerization rates were measured as the sum of the dimer (butene) and trimer (hexene) formation rates, considering trimerization to occur in series with dimerization. Steady-state, condensed-phase ethene dimerization rates were measured at 243 and 253 K above the ethene pressures of 12 bar and 18 bar that respectively cause condensation of intrapore liquid ethene and attenuated catalyst deactivation,⁵⁶ while pseudo-steady-state gas-phase ethene dimerization rates were measured at 243 and 253 K below these threshold ethene pressures and led to catalyst deactivation. Pseudo-steady-state rates were measured after 5 h of reaction time at 448 K when deactivation was less rapid than at initial reaction times. [NiOH]+ were proposed to be the active sites on Ni-MCM-41 because steady-state rates (243 K and 15 bar C₂H₄, per g_{cat}) increased linearly with Ni content until each H⁺ initially present on the MCM-41 support was exchanged with Ni, and were independent of Ni content thereafter. In order to account for the non-ideal character of the gas phase during steady-state condensed-phase oligomerization (243 K and >12 bar C₂H₄, 253 K and >18 bar C₂H₄) by transition state theory, ethene pressures were converted into gas-phase fugacities, and the non-ideality of transition states was accounted for by estimating their activity coefficients (γ^{\dagger} < 1) within intrapore liquid ethene. Such corrections for transition state non-ideality were not required to interpret rates measured under gas-phase conditions. Steady-state rates (243, 253 K) for condensed-phase oligomerization and the pseudosteady-state rates (243, 253, 448 K) for gas-phase oligomerization showed a second-order dependence on ethene fugacities and pressures (5-25 bar), respectively, indicating predominantly uncovered Ni active sites. 56 The pseudo-steadystate rate for gas-phase dimerization measured at 448 K and 15 bar ethene pressure was ~55% lower than that measured during initial reaction time, reflecting dimerization turnovers on only a fraction of Ni sites.56

In the case of Ni-MCM-41, the effect of Ni content on measured alkene oligomerization rates has also been reported. Propene oligomerization rates were taken as propene consumption rates (per Ni, 453 K) on a series of Ni-MCM-41 samples after air treatment (773 K, 3 h).⁷⁷ All Ni-MCM-41 samples deactivated with reaction time and oligomerization rates did not stabilize during (~6.25 h) the experiment.⁷⁷ For Ni-MCM-41 samples with the same Si/Al ratio (~20), propene oligomerization rates (per Ni) were consistently lower for

samples with increasing Ni content (0.3-1.1 wt.%) throughout the experiment. Transient propene oligomerization rates were lower for samples with decreasing Si/Al ratio (37-12) that contained similar amounts of Ni (0.90 ± 0.13 wt. %). These results were summarized by comparing oligomerization rates measured at ~6.25 h for all the samples as a function of Ni areal density (Ni nm⁻²), as shown in Figure 1. Propene oligomerization rates (per Ni, 453 K) decreased with increasing the areal density of Ni sites (Ni nm⁻²), when measured on partially deactivated samples at a fixed reaction time during transient experiments (Fig. 1). Propene oligomerization rates (per Ni), however, did not show a monotonic trend with Ni/Al among all Ni-MCM-41 samples, which may reflect that each Ni-MCM-41 sample did not deactivate to the same extent over the same reaction time (6.25 h). Nevertheless, these results suggest that propene oligomerization rates (per Ni active site) may be influenced by the density of Ni sites on MCM-41 supports, which is a kinetic detail that remains incompletely understood.

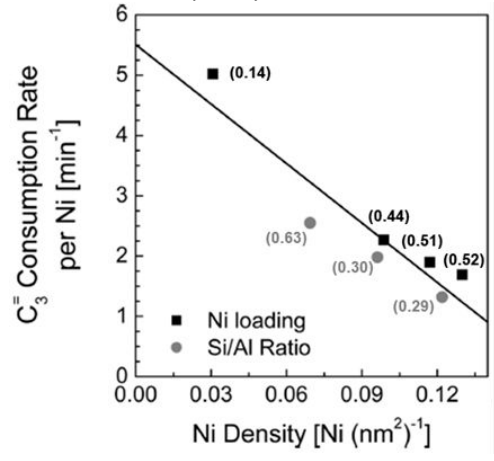


Fig. 1 Effect of Ni surface density (Si/Al =10–40; Ni = 0.3–1.13 wt.%) on propene consumption rate for Ni-Na-MCM-41 at 453 K, 1 bar propene and measured at approximately 6.25 h of time on stream. The numbers in parenthesis indicate the approximate Ni/Al ratio. (reproduced with permission from Mlinar et al.⁷⁷)

4.2 Kinetics on Ni-MOFs

Kinetic studies on Ni-MOFs typically use batch or semi-batch reactors, however, catalytic rates determined by fitting timeresolved data with appropriate reactor model equations have rarely been reported. Instead, a common approach in these studies has been to report so-called "turnover frequencies" (TOF) determined by quantifying the cumulative amount of reactant consumed (or the oligomer products formed) after the reactor has been quenched, and normalizing by the total number of Ni present in the reactor via the Ni-MOF. Such TOF values represent time-averaged reaction rates over the duration of the experiment, and not the intrinsic rate of alkene chain growth on Ni-MOFs, preventing their rigorous comparison among experiments performed for different times or with different protocols (e.g., for co-catalyst activation).86 Some Ni-MOFs (e.g., Ni-AIM-NU-1000⁶⁵) have been tested in a continuous flow reactor for gas-phase alkene reactions and corresponding kinetic analyses have been reported.

Measured time-averaged rates of alkene chain growth reactions on Ni-MOFs are reported to be significantly influenced by the relative amount of co-catalyst (or activator), commonly expressed as the Al/Ni ratio, charged to the reactor to initiate the reaction. Time-averaged ethene oligomerization rates (298 K, 50 bar C₂H₄, toluene) on Ni-MFU-4l increased from 5,900 h⁻¹ to 21,000 h⁻¹ upon increasing the co-catalyst (MAO) charge from an Al/Ni of 50 to 100, but increased to only 27,000 h⁻¹ at an Al/Ni of 500.52 Time-averaged ethene oligomerization rates (295 K, 50 bar C₂H₄, toluene) on Ni-CFA-1 increased monotonically from 13,100 to 36,300 h⁻¹ with increasing co-catalyst (MMAO-12) charge from an Al/Ni of 50 to 1,000.88 Time-averaged ethene oligomerization rates (298 K, 30 bar C₂H₄, heptane) on Ni@(Fe)MIL-101 increased from 3,000 h-1 to 10,500 h-1 with increasing co-catalyst (Et₂AlCl) charge from an Al/Ni of 20 to 70, but did not increase above an Al/Ni of 70.62 On the other hand, time-averaged ethene oligomerization rates (323 K, 10 bar C₂H₄, cyclohexane) on Ni@(Ti)MIL-125 increased from 0.73 to 1.81 g (mol Ni)⁻¹ h⁻¹ with increasing co-catalyst charge (MAO) from an Al/Ni of 100 to 800, but decreased to 1.53 g (mol Ni)-1 h-1 as the Al/Ni increased to 1500, hypothesized to reflect over-reduction of precursor Ni sites.87 Taken together, these findings indicate that the fraction of Ni precursor sites that are converted into the active sites for alkene chain growth reactions depend on the co-catalyst charge, but trends cannot be generalized among Ni-MOFs or co-catalysts of different identity.

The dependence of time-averaged alkene chain growth rates on Ni-MOFs on alkene pressure has also been investigated at a fixed co-catalyst charge, given the aforementioned effects of co-catalyst charge. Time-averaged ethene oligomerization rates (298 K, toluene, MAO Al/Ni = 100) measured on a 10 wt.% Ni-MFU-4l sample showed an apparent first-order dependence on ethene pressure up to 25 bar, followed by an apparent zeroorder dependence between 25 and 50 bar.⁵² In the case of Ni-CFA-1, which contains node structures structurally homologous to Ni-MFU-4I, time-averaged ethene oligomerization rates (295 K, toluene, MAO Al/Ni = 100) showed an apparent first-order dependence on ethene pressure up to 50 bar, without a transition to a zero-order regime. The apparent first-order dependence on ethene pressure for Ni-MFU-4I and Ni-CFA-1 is attributed to the prevalence of coordination-insertion mechanism on a [Ni(II)-ethyl]+ active site, implying the [Ni(II)ethyl]+ species as the predominant reaction intermediate and ethene insertion into the [Ni(II)-ethyl]+ as the sole rate limiting step.

The effect of Ni loading within Ni-MOFs on the alkene chain growth rates has also been investigated at a fixed co-catalyst charge. Time-averaged ethene oligomerization rates per Ni (298 K, 50 bar C₂H₄, toluene, MAO at Al/Ni=100) measured on Ni-MFU-4l samples containing varying fractions (1, 3, 10, 30 mol. %) of their Zn nodes exchanged with Ni showed an approximate linear decrease with increasing Ni content, proposed to reflect mass transport limitations after assuming that deactivation was absent.⁵² The Ni-MFU-4l sample with 1 mol. % Ni showed a time-averaged rate (per Ni) of 41,000 h⁻¹ that was comparable to the maximum time-averaged rate observed on the analogous homogeneous catalyst, [Tp^{Mes}Ni]⁺, suggesting that the Ni active

structures in a Ni-MFU-4l sample containing dilute Ni may indeed function as a heterogeneous version of the molecular catalyst.⁵² Unlike Ni-MFU-4l, Ni-CFA-1 samples with varying Ni content (1 and 7.5 mol. %) did not show different time-averaged ethene oligomerization rates (per Ni) (295 K, 10-50 bar C_2H_4 , MMAO-12 at Al/Ni=1000),88 even though the precursor Ni site structures are structurally analogous within these MOFs. This likely reflects the 10× excess co-catalyst charge in the Ni-CFA-1 (Al/Ni=1000) study⁸⁸ as compared to the Ni-MFU-4l (Al/Ni=100) study,⁵² which ensured that nearly all precursor Ni sites were converted into active sites irrespective of the Ni content in the MOF. Similarly, Ni@(Fe)MIL-101 samples were prepared with 10% and 30% of their 2-aminoterephthalate organic linkers functionalized to contain the organometallic Ni precursor sites, and showed similar ethene oligomerization rates (per Ni, 283 K, 15 bar C₂H₄, heptane, Et₂AlCl at Al/Ni=70).⁶² These examples demonstrate the challenges in studying the effect of Ni content on ethene dimerization rates when using a constant charge of co-catalyst, because the specific amounts of co-catalyst required (even at stoichiometric excess) to fully convert all precursor Ni sites to coordination-insertion active sites varies with the Ni content of the MOF.

Rates of alkene chain growth reactions have also been shown to depend on the organic solvent used, as well as the reaction media (gaseous or solvent). The influence of solvent type on ethene oligomerization rates is evident in the case of Ni@(Ti)MIL-125, wherein cyclohexane and toluene were used as organic solvents.87 Time-averaged ethene oligomerization rates (323 K, 10 bar C₂H₄, MAO at Al/Ni = 800) measured on Ni@(Ti)MIL-125 were 50% lower when using toluene instead of cyclohexane,87 however, the mechanistic origins for this effect were not explored and this remains an empirical observation. The effect of solvent type on reaction rates has not been explored for all Ni-MOFs, and it remains unclear if solvent identity influences the transformation of Ni precursor sites into the Ni active site structures or the intrinsic turnover rates at these sites. The influence of organic solvent on ethene dimerization rates was demonstrated for Ni-NU-1000-bpy, by performing reactions in heptane and in the gas-phase. Ni-NU-1000-bpy solids were first activated with Et₂AlCl (Al/Ni = 70) in a heptane solution and time-averaged ethene dimerization rates (ambient temperature) were measured by subjecting the activated solids to a constant ethene pressure (15 bar) in a semibatch reactor for 1 hour. An identical experiment in the gas phase involved first activating Ni-NU-1000-bpy solids with Et₂AlCl (Al/Ni = 70) solution in heptane, isolating the solids, washing with heptane solvent, and drying them prior to contact with 15 bar of gaseous ethene. Time-averaged ethene dimerization rates (ambient temperature, 15 bar C_2H_4) were ~28× times lower in the gas-phase than in solvent, however, rates in the gas-phase on Ni-NU-1000-bpy solids crushed into a fine powder increased to ~80% of those in heptane solvent. The products formed in these reactions were predominantly dimers (>90%), but gas-phase reaction also formed ~20% trimers and tetramers, which suggested that the organic solvent enhances the desorption of dimers and thus their extraction from the MOF pores to prevent subsequent chain growth events.

Mini review

Rates of alkene chain growth reactions in the gas phase have also been measured in a continuous flow reactor on Ni-AIM-NU- $1000.^{65}$ Ni-AIM-NU-1000 was activated with Et₂AlCl (Al/Ni = 70) solution in heptane using the same procedure described above for Ni-NU-1000-bpy,61 and the dried solids were contacted at 318 K with 2 bar ethene in a fixed-bed continuous reactor. Ni-AIM-NU-1000 deactivated with reaction time and reached a pseudo steady-state after 10 h on stream with the pseudosteady-state oligomerization rate being 80% lower than that at initial time. Unlike time-averaged rates estimated from batch and semi-batch reactor studies, these pseudo steady-state rates reflect the instantaneous rates of coordination-insertion cycles, although only on a minority of Ni sites that remain active after 10 h of deactivation. Pseudo-steady-state ethene consumption rates (312-354 K) measured under differential conversion conditions (<10%) showed an apparent activation energy of 35 kJ mol⁻¹, although the apparent reaction order was not determined.65

5. Mechanistic considerations for the product selectivity of alkene chain growth reactions

5.1 Product selectivity on Ni-based microporous and mesoporous inorganic supports

Ni based microporous and mesoporous inorganic materials predominantly form alkene dimers as primary products during chain growth reactions of ethene,56,78,93,94 propene49,77,95 and 1-butene.55, 96 This tendency to prefer chain termination over propagation resembles that of numerous homogeneous Ni catalysts.7, 9, 97, 98 Depending on the reaction conditions and conversion, trimers, tetramers and higher oligomers of the reactant alkene are also formed by subsequent homo- or hetero-dimerization events. Given the prevalence coordination-insertion catalytic cycles on these materials, product chain lengths depend on the relative rates of chain propagation and termination. In the case of product mixtures containing true oligomers, the carbon selectivity of the oligomers can be suitably described by statistical Schulz-Flory distributions ($C_{2n} > C_{3n} > C_{4n}$... for a C_n alkene). 99 In the case of ethene chain growth reactions, Ni-based porous inorganic materials are reported to yield a Schulz-Flory distribution of products at temperatures below 423 K and ethene pressures above 30 bar, 46 while non-Schulz-Flory product distributions are obtained at temperatures above 423 K as contributions from side-reactions on residual H⁺ sites become more significant.^{2, 3,}

The linear dimer products formed on these Ni inorganic materials consist of a mixture of double-bond (positional) isomers. The assessment of double-bond isomerization pathways on Ni sites is convoluted by the presence of residual H $^+$ sites in the case of aluminosilicate supports. In order to distinguish between double-bond isomerization pathways that occur on the Ni and H $^+$ sites, ethene oligomerization (453 K, 0.2 kPa C₂H₄) was studied on H-Beta and a control sample of Ni-Beta that contained no residual H $^+$ sites detectable by *ex-situ*

characterization.33 The H-Beta sample showed evidence of double-bond isomerization on H⁺ sites to form an equilibrated mixture of 1-butene, cis-2-butene and trans-2-butene, which was accompanied by skeletal isomerization to form isobutene; thus, isobutene was identified as a kinetic marker of the presence of H⁺ sites and, in turn, double-bond isomerization also occurring at such sites. Rates of isobutene formation on H-Beta decrease with time-on-stream as H⁺ sites deactivate. An identical experiment on the control Ni-Beta sample formed only traces of isobutene that disappeared with reaction time as residual H⁺ sites deactivated, after which 1-butene and 2butene isomers were formed at steady-state in nonequilibrated ratios.33 These results show that double-bond isomerization pathways are catalyzed at Ni active sites, consistent with the coordination-insertion mechanism (Scheme 2a).³³ Further, 1-butene, cis-2-butene, and trans-2-butene were formed as primary products because variations in sitecontact time showed that the non-equilibrated product distribution among these positional isomers remained invariant under differential ethene conversions (<1%).33

Another study⁴⁷ measured the yields of linear butene isomers on Ni-H-Beta (393 K, 17.4 bar C₂H₄, 29 bar total pressure) as a function of ethene conversion at pseudo-steadystate (after 10 h time-on-stream) following a deactivation period. Measured yields of 1-butene, cis-2-butene and trans-2butene increased linearly with ethene conversion (0-15%), and in non-equilibrated ratios that were invariant with conversion, indicating the linear butene isomers were primary products formed at Ni sites.⁴⁷ Similarly, for ethene oligomerization (423 K, 4 bar C₂H₄ (26 bar inert) or 18 bar C₂H₄ (12 bar inert)) on Ni-AFI,58 linear butene isomer yields were measured after isobutene was no longer detected at long reaction times (>16 h), and increased linearly with conversion (0-8%) in nonequilibrated amounts, also providing evidence that linear butene isomers are primary products formed at Ni sites.⁵⁸ These data highlight a characteristic of the coordination-insertion mechanism wherein [Ni(II)-1-alkyl]⁺ intermediates can isomerize to form [Ni(II)-2-alkyl]⁺ intermediates prior to alkene desorption (Scheme 2, 5a conversion to 5c), forming a mixture of terminal and internal linear alkene products. Accordingly, the ratio of 1-butene to 2-butenes on Ni-AFI⁵⁸ extrapolated to finite values at zero conversion, representing the composition of linear butenes dictated by the coordination-insertion mechanism at the Ni sites present on this support. The initial 1-/2-butenes ratio was significantly higher at 18 than at 4 bar ethene pressure,⁵⁸ indicating that higher ethene pressures favor β -hydride elimination of 1-butene from [Ni(II)-1-butyI]⁺ intermediates (i.e., chain transfer steps to reactant ethene monomers) over isomerization into [Ni(II)-2-butyl]+ species (Scheme 2a).9 The non-equilibrated product alkene distributions formed, and their dependence on reactant alkene pressure, reflect kinetic control over the positional isomerization selectivity upon a single sojourn at an active Ni site in the coordination-insertion mechanism.

Scheme 9 Sequence of alkene insertion modes into a metal-hydride bond that influence the molecular structure (branched vs. linear) of the alkene dimer; (a) 1,2- and 1,2-; (b) 1,2- and 2,1-; (c) 2,1- and 1,2-; and (d) 2,1- and 2,1-. (reproduced with permission from Nicholas, C.P.¹⁴).

The selectivity among terminal and internal isomers of dimer products has also been reported to vary with alkene conversion. During ethene oligomerization on Ni-AFI⁵⁸ (423 K) at long reaction times (>16 h), the selectivity to 1-butene among linear butene isomers decreased with increasing conversion (0-8%), but did not reach an equilibrated composition, indicating double-bond isomerization occurring via re-adsorption of 1butene on Ni sites. At iso-conversion (~2%), the 1-butene selectivity was >2× higher at 18 bar than 12 bar ethene pressure,⁵⁸ suggesting that re-adsorption of 1-butene on Ni sites was hindered by higher ethene coverages at Ni sites at higher pressures. Similarly, for gaseous ethene oligomerization (448 K) on Ni-MCM-41⁵⁶ at pseudo-steady-state (>5 h time-onstream), the selectivity to 1-butene among linear butene isomers decreased with increasing ethene conversion (0-10%) for samples with varying Ni content (Ni²⁺/H⁺_{initial} = 0.1-5.0).⁵⁶ Ni-MCM-41 samples with higher fractions of H⁺ sites showed more rapid decreases in 1-butene selectivity with time-on-stream, suggesting faster rates of butene isomerization on H+ than Ni sites at 448 K. In the case of both Ni-AFI and Ni-MCM-41 samples, the 1-butene selectivity was <100% when extrapolated to zero conversion, highlighting that double-bond isomerization occurs at Ni sites prior to alkene desorption, in addition to the secondary isomerization pathways on H⁺ and Ni sites upon re-adsorption of butene products. The 1-butene selectivity on Ni-MCM- 41^{56} samples (Ni²⁺/H⁺_{initial} = 0.1–5.0) in the presence of intrapore liquid ethene (243 K, 15 bar C₂H₄), however, decreased with conversion identically for all samples irrespective of their relative amounts of Ni and H⁺ sites, and

extrapolated to 100% at zero conversion.56 This indicated that

secondary isomerization (at 243 K) occurred only at Ni sites but

not H⁺ sites, and that isomerization pathways at Ni sites were

inhibited, which was attributed to the preferential solvation of

later transition states for 1-butene desorption than the earlier

transition states for 1-butene isomerization or chain growth.^{56,}

The positional isomerization of linear alkenes is also influenced by co-cations on aluminosilicate supports. The dimerization of 1-butene on Ni-Ca-LTA is accompanied by parallel isomerization of 1-butene into 2-butenes involving $\pi\mbox{-}$ allyl bound butene and Ni-alkyl intermediates observed by IR spectroscopy.55 Non-catalytic alkali (Li+) and alkaline earth (Mg²⁺) cations were exchanged into Ca-LTA zeolite and showed no isomerization of 1-butene (50 bar) in the absence of Ni2+ at 433 K.96 With Ni2+ present, however, Ni-Ca-LTA, Ni-Mg-Ca-LTA and Ni-Li-Ca-LTA formed linear butene isomers that approached an equilibrated distribution (433 K) with increasing 1-butene conversion (extrapolated to initial time). In otherwise identical experiments, values of the 1-butene conversion corresponding to the formation of equilibrated butene mixtures depended on co-cation identity in the order Ca > Mg > Li, indicating the relative rates of isomerization were higher on Ni-Li-Ca-LTA > Ni-Mg-Ca-LTA > Ni-Ca-LTA.96 These observed effect of Li and Mg corresponded to their higher Sanderson electronegativity relative to Ca, hypothesized to stabilize the π -allyl bound butene intermediate and result in higher rates for double-bond isomerization.96 In the case of propene dimerization (453 K, 5 bar C₃H₆) on Ni-X zeolites with non-catalytic alkali (Li, Na, K) and alkaline earth (Mg, Ca, Sr) co-cations, however, the distribution between terminal and internal isomers of dimer products measured at pseudo-steady-state was independent of co-cation identity.95 Thus, the specific mechanistic details regarding the effects of non-catalytic co-cations on alkene double-bond isomerization at Ni active sites remain unclear.

The selectivity between branched and linear dimer products is also mechanistically controlled by the sequence of coordination and insertion events of the alkene monomer. Schemes 9a-d shows four possible sequences of coordination-insertion events for an asymmetric alkene at the Ni active site.

The reactant alkene can insert into the Ni-hydride (Ni-H) bond in two ways, namely 1,2- and 2,1- insertions, and the possible sequences of these insertion events leads to linear (Scheme 9b), mono-branched (Scheme 9a, d) or di-branched (Scheme 9c) isomers of the dimer. In the case of a symmetric alkene, however, the 1,2- and 2,1- insertions are indistinguishable and thus will form identical dimers in each of the four sequences.

The selectivity between linear and branched dimers during alkene chain growth reactions at exchanged Ni2+ cations in microporous and mesoporous inorganic supports has been altered by structural modifications. The effect of non-catalytic alkali (Li, Na, K) and alkaline earth (Mg, Ca, Sr) co-cations exchanged in Ni-X zeolites on branching in dimer products was studied for gas-phase propene oligomerization (453 K, 5 bar C₃H₆).⁹⁵ Figure 2 shows the degree of dimer branching, defined as a percentage ratio of the sum of mono- and di-branched dimers to linear dimers, as a function of the free volume per FAU supercage. The degree of dimer branching was higher for all alkaline earth co-cations than for alkali co-cations (Fig. 2), attributed to preferential siting of alkali co-cations in the supercage that increased the steric constraints for propene dimerization. Additionally, the degree of dimer branching followed the order Li (smallest cation) > Na > K among alkali metals, and Sr (largest cation) > Ca > Mg among alkaline earth metals, increasing with the free volume per supercage in both cases.95 It was hypothesized that the larger volume available around Ni sites in the FAU supercage stabilized the reactive intermediates formed by 2,1-insertion leading to the observed selectivity towards branched dimers.95 Similarly, the degree of dimer branching for propene oligomerization (453 K, 1 bar C₃H₆) was examined in the case of Ni-MCM-41 samples with various non-catalytic alkali co-cations (Li, Na, K, Cs).⁷⁷ In this case, the degree of dimer branching was unaffected (47-49 %) by alkali identity, suggesting a less significant effect of changing the free volume around Ni active sites by the alkali in Ni-MCM-41 than in Ni-X zeolites.⁷⁷ This difference in the observed effects of cocations on dimer branching between Ni-X and Ni-MCM-41 was rationalized by suggesting that branching is influenced by electronic effects induced by the proximity between the noncatalytic co-cations and Ni active sites.77

The effect of non-catalytic alkali (Li+) and alkaline earth (Mg²⁺, Ca²⁺) metal co-cations on branching in dimer products was also studied for 1-butene oligomerization (453 K) on Ni-LTA. The ratio of branched to linear dimer products was influenced by the extent of double bond isomerization of 1-butene to 2butene in the feed. Considering 1-butene as the sole reactant for the insertion sequences described in Scheme 9, a linear dimer can be only formed for 1,2-insertion followed by 2,1insertion (Scheme 9b), while any other combination leads to a dimer with at least one branch. In contrast, with 2-butene as the sole reactant, all insertion sequences (Scheme 9a-d) form 3,4dimethyl-2-hexene, a di-branched dimer. While considering 1butene and 2-butenes as the alternating reactants in each of the two insertion steps (Scheme 9), all possible combinations of insertion sequences form a dimer with at least one branch. These mechanistic considerations imply that greater extents of

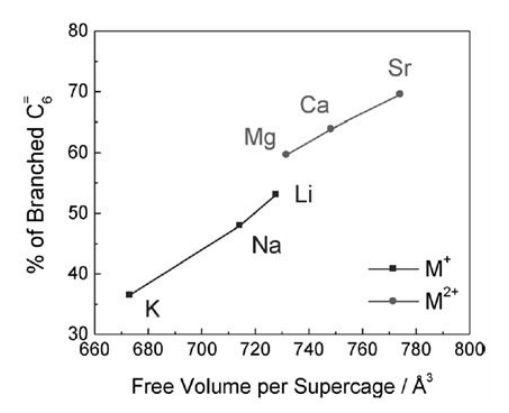


Fig. 2 Percentage of branched isomers (containing at least one methyl branch) within the dimer fraction of propene oligomerization products as a function of free volume of FAU supercage measured on Ni-M-X (M = Li, Na, K, Mg, Ca or Sr) at 453 K, 5 bar propene and 2 h of time-on-stream after initial deactivation (adapted with permission from Mlinar, A.N. et al.^{77, 95}).

1-butene double-bond isomerization to 2-butenes will result in higher fractions of branched dimer products. Accordingly, for Ni-LTA, the selectivity toward branched dimers followed the same trend as that for the rate of double-bond isomerization, in the order Ni-Li-Ca-LTA < Ni-Mg-Ca-LTA < Ni-Ca-LTA. ⁹⁶

5.2 Product selectivity on Ni-MOFs

Alkene chain growth reactions on most reported Ni-MOFs predominantly form alkene dimers⁷² analogous to homogeneous organometallic^{7, 97, 98} and inorganic porous Ni catalysts,^{2, 3} consistent with the tendency of Ni to favor chain termination over propagation.9 In the case of some Ni-MOFs, such as Ni-AIM-NU-1000⁶⁵ preactivated with Et₂AlCl (Al/Ni = 70) as in the case of Ni-NU-1000-bpy⁶¹ (Section 4.2), gas-phase ethene oligomerization (318 K, 0.2 bar C₂H₄) showed 48% dimers, 8% trimers and 46% tetramers at 5% conversion after an initial deactivation over 10 h. Also, in the case of ethene oligomerization on Ni@(Ti)MIL-12587 (323 K, 10 bar C_2H_4 , cyclohexane, Al/Ni = 800), trimers and tetramers were formed in comparable amounts to dimers, and the product composition (C_4 , C_6 , C_8 , $\ge C_{10+}$) varied with co-catalyst identity including MAO (20%, 77%, 1%, 2%), Et₃AlCl (49%, 48%, 1.5%, 1.5%), Et₂AICI (68%, 30%, 1%, 1%) and EtAICI₂ (58%, 39%, 2%, 1%). These examples suggest that the carbon selectivity of alkene oligomerization products depends on the specific Ni-MOF catalytic system (Ni-MOF, solvent, co-catalyst).

Structural modifications of Ni-MOFs are also reported to affect the carbon selectivity of products during alkene chain growth reactions. NU-1000 was modified with stronger electron withdrawing ligands, hexafluoroacetylacetonate (Facac¹) and acetylacetonate (acac¹), followed by installation of Ni(II) structures via ALD-type techniques to form Ni-Facac-NU-1000 and Ni-Acac-NU-1000, respectively. 100 The unmodified Ni-AIM-NU-1000, Ni-Facac-NU-1000 and Ni-Acac-NU-1000 samples were activated with Et₂AlCl (Al/Ni = 70) solution in heptane using the same procedure as described before (Section 4.2) for Ni-NU-1000-bpy, 61 and the dried solids were contacted at 318 K with 2 bar ethene in a fixed-bed continuous reactor. The product selectivities measured at pseudo-steady-state after 10 h of deactivation and under differential ethene conversions (<3%) are shown in Figure 3, indicating selective formation of

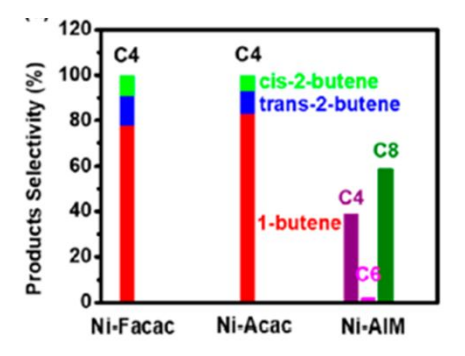


Fig. 3 Product distribution of ethene oligomerization on Ni-Facac-NU-1000, Ni-acac-NU-1000, and Ni-AlM-NU-1000 activated with Et₂AlCl (Al/Ni=70) at 318 K and 2 bar ethene (adapted with permission from Liu et al. 100).

butenes for Ni-Facac-NU-1000 and Ni-Acac-NU-1000, while the Ni-AIM-NU-1000 formed butenes (dimer), hexenes (trimer), and octenes (tetramer). These differences in the product selectivity were explained by DFT (M06-L, Gaussian 09) showing that activation free energies were higher for trimerization than for dimerization by 40 and 49 kJ mol⁻¹ for Ni-Facac-NU-1000 and Ni-Acac-NU-1000, respectively, whereas activation free energies were comparable for Ni-AIM-NU-1000. The higher free energy barriers were concluded to arise from siting of Facac and Acac ligands, resulting in partial ligation with the Ni center. 100

Alkene pressures have been shown to influence the carbon selectivity and positional isomerization of linear dimers on Ni-MOFs. In the case of ethene oligomerization (298 K, toluene, MAO Al/Ni = 100) on Ni-MFU-4l,⁵² butenes were predominant products and small amounts of hexenes were also produced. As ethene pressure increased from 5 to 50 bar, the selectivity to 1butene increased from 73% to 95%, while that for hexenes decreased from 7% to 3%. Higher ethene pressures were proposed to inhibit the re-insertion of 1-butene into [Ni(II)ethyl]+ sites, thus preventing their subsequent isomerization to 2-butene isomers and secondary insertion to form [Ni(II)-hexyl]+ intermediates to yield hexenes. By further optimizing the reaction conditions (273 K, 50 bar C₂H₄, toluene, MAO Al/Ni = 100), a 1-butene selectivity of 96% was obtained on Ni-MFU-4l, which is higher than the 81% selectivity obtained on the analogous homogeneous [TpMesNi]+ complexes.52 This result was attributed to sterically less hindered Ni sites in Ni-MFU-4l that enhance rates of β -hydride elimination relative to chain isomerization and propagation. The effect of increasing ethene pressure from 5 to 50 bar during ethene oligomerization (295 K, toluene, MMAO Al/Ni = 1000) showed a similar result on Ni-CFA-188 (which contains Ni structures analogous to Ni-MFU-4I), wherein the 1-butene selectivity increased from 75% to 86% and the hexene selectivity decreased from ~8% to ~3. Similar results were also obtained for ethene oligomerization (293 K, toluene, Et₂AlCl Al/Ni = 100) on NiMixMOF⁶⁴ with increasing pressure from 20 to 30 bar, which increased butene selectivity from 80% to 92%, and a decrease in hexene and octene selectivity from 7% to 3% and 13% to 5%, respectively.

Reaction temperature also influences the carbon selectivity and positional isomerization of linear dimers during ethene oligomerization on Ni-MFU-4l52 and Ni-CFA-1.88 With increasing reaction temperature from 273 K to 323 K, ethene oligomerization (50 bar C₂H₄, toluene, MAO Al/Ni = 100) on Ni-MFU-4l showed a decrease in 1-butene selectivity from 98% to 88%, while the hexene selectivity increased from 2% to 12%.52 Similarly, for Ni-CFA-1 (50 bar C₂H₄, toluene, MMAO-12 Al/Ni = 1000), the 1-butene selectivity decreased from 98% to 81%, while the hexene selectivity increased from 2% to 7% as the reaction temperature increased from 273 K to 323 K.88 These results were attributed to a decrease in ethene concentration in the solvent and the entropic preference for the isomerization [Ni(II)-1-alkyl]+ intermediates into [Ni(II)-2-alkyl]+ intermediates over β -hydride elimination to desorb 1-butene during coordination-insertion cycles.88

The effect of reaction medium on the product selectivity was explored for ethene oligomerization on Ni-NU-1000-bpy.61 Ethene oligomerization (ambient temperature, 15 bar C2H4, Et₂AlCl Al/Ni=70) on Ni-NU-1000-bpy in heptane solvent showed products to consist of 93% butenes and 7% hexenes and octenes, with the linear butenes comprised of 91% 1butene. 61 An identical gas-phase experiment after activating Ni-NU-1000-bpy with Et₂AlCl (as described in Section 4.2), produced 83% butenes and 16% hexenes and octenes, with the linear butenes comprised of 85% 1-butene. Further, reaction in the gas phase on activated and crushed Ni-NU-1000-bpy solids showed similar time-averaged rates as reactions performed in a solvent, and produced 82% butenes and 18% hexenes and octenes, with the linear butenes comprised of 57% 1-butene.61 The lower selectivity for 1-butene and the higher selectivity for hexenes and octenes in the gas-phase reaction was hypothesized to reflect the absence of organic solvent, leading to higher local concentrations of 1-butene within Ni-NU-1000bpy pores favoring secondary isomerization and chain growth reactions.61

The selectivity between linear and branched oligomers during alkene chain growth reactions on Ni-MOFs has not been extensively studied, although propene dimerization on Ni-MFU-4l⁶⁰ provides some mechanistic insights. Propene dimerization (294 K, 6 bar C_3H_6 , MMAO-12 Al/Ni = 500) was carried out on Ni-MFU-4l in C_6D_6 solvent allowing the resulting product distribution to be quantitatively analyzed by ¹³C NMR. The resulting dimer products consisted of ~76% branched dimers and 26% linear dimers. The product distribution was parsed into insertion sequences (Scheme 9) based on the quantitative analysis of each chain isomer of hexene, showing a mechanistic preference for 2,1-insertion over 1,2-insertion of propene. This analysis indicated that the preference for 2,1-insertion over 1,2-insertion of propene (regioselectivity) increases with the steric size of alkyl group on Ni(II) (H < 1-propyl < 2-propyl).

6. Conclusions and outlook

The experimental^{33, 54} and computational³⁸ studies discussed here highlight mechanisms wherein exchanged Ni²⁺ cations on inorganic porous supports can transform *in situ* via

Mini review

elimination of 1,3-butadiene and formation of proximal H⁺ sites to form the coordination-insertion active sites, in the absence of externally supplied activators or co-catalysts, in a manner analogous to some Ni-homogeneous^{36, 37} catalysts that also operate in the absence of co-catalysts. For $[Ni(II)OH]^+$ precursor sites on inorganic porous supports, two mechanistic pathways involving elimination of either ethenol³⁸ or water⁵⁸ have been proposed, however, only the former is supported by DFT calculations, while neither have been validated by experiments. Further research to identify different candidate Ni precursor structures and the mechanisms to convert them into coordination-insertion active sites will help continue developing strategies to form metal-hydride and metal-alkyl sites in the absence of externally supplied alkyl-transfer agents. In the case of Ni-MOFs, coordination-insertion active sites are formed in the presence of alkylaluminum co-catalysts by a mechanism similar to that of homogeneous Ziegler-Natta polymerization catalysts, but the practical use of Ni-MOFs is challenged by activation procedures that require organic solvents and large stoichiometric excesses of pyrophoric alkylaluminum compounds. Recently, some Ni-MOFs (e.g., UiO-67,73 Ni-MOF-74⁷²) have been reported to catalyze gas-phase alkene chain growth reactions in the absence of external activators, albeit at turnover rates significantly lower than Ni-MOFs with external activators. Additional mechanistic understanding can help design Ni-MOFs that can be activated without alkylaluminum compounds to form Ni active sites that function as molecular catalysts with high turnover rates.

Experimental studies^{47, 79} have proposed that deactivation of microporous aluminosilicates containing both Ni2+ and H+ sites is caused by forming heavier oligomers, polyconjugated aliphatic compounds or polycondensed aromatics that are purported to more strongly adsorb at active sites and block porous voids. Ni-exchanged microporous supports without residual H⁺ sites also deactivate during alkene chain growth reactions, 33, 49 however, possibly indicating that H+ sites formed in situ during formation of the coordination-insertion active Ni sites might play a role in deactivation, or that deactivation mechanisms at Ni sites also occur independent of the relative amounts of H+ sites initially present on the support. Further research is needed to clarify the mechanistic connections between the deactivation of exchanged Ni2+ and residual H+ sites on microporous inorganic supports. Moreover, the multisite deactivation of exchanged Ni²⁺ cations in these materials is purported to reflect their mobile nature under reaction conditions,⁴⁹ and further experimental (e.g., EXAFS) and theoretical studies are required to validate this model. Further, the deactivation of various Ni-containing microporous supports indicates a multi-site deactivation mechanism, while that of mesoporous supports with significantly lower Ni spatial density indicates a single-site mechanism. Although the effects of Ni spatial density on deactivation appears consistent between microporous and mesoporous materials, the mechanistic origins for these differences and how Ni density influences the deactivation mechanism within each class of porous supports is unknown.

Deactivation was further shown to be inhibited in the presence of intrapore liquid ethene in Ni-MCM-41,⁵⁶ consistent with another study⁸⁵ suggesting solvent-like properties of liquid alkenes inhibit deactivation during chain growth reactions. Ethene chain growth reactions on Ni-MCM-41 in heptane solvent in a three-phase slurry semi-batch reactor, however, lead to deactivation.81 Yet, slurry reactors that operate under the liquid-like conditions provided by condensed oligomer products at high pressures have been shown to favor longer catalyst lifetimes during ethene oligomerization on Ni/SiO₂-Al₂O₃, 101 motivating further research focused on the role of organic solvents on catalyst deactivation and stability. The deactivation of Ni-MOFs has been generally attributed to formation of polymeric deposits, or adsorbed oligomers and activators at active sites, and has been mechanistically investigated in the case of Ni-MFU-4I, where it was attributed to reductive demetallation. The regeneration protocols for Ni-MOFs to promote their reuse, however, have generally not been mechanistically investigated. Although Ni-MOFs have been hypothesized to show greater stability in a solvent than in the gas phase, the specific roles of solvents on the deactivation of Ni-MOFs has not been fully explored.

Kinetic measurements for alkene chain growth reactions on Ni-containing inorganic supports under deactivating conditions are typically reported at pseudo-steady-state conditions, and thus probe catalytic turnovers on only a fraction of Ni sites. In most cases, kinetic analysis is based on net product formation rates, and not their forward rates of formation. These rates (per Ni) are also influenced by the density of Ni sites within porous inorganic supports. Time-averaged rates of alkene chain growth measured on Ni-MOFs are influenced by the co-catalyst used, the amount of co-catalyst charged, the reaction media (gaseous or solvent) and the type of organic solvent used as the reaction medium. Additionally, the specific influence of these factors on the alkene chain growth rates varies with the structural composition of Ni-MOFs, however, not all of these factors have been explored for each Ni-MOF. A more rigorous assessment of kinetic data by determining initial forward reaction rates, normalized by the fraction of Ni sites that form active intermediates in coordination-insertion cycles, will aid in determining the intrinsic turnover rates for alkene chain growth reactions. Such data would clarify the structural requirements of various Ni precursor sites proposed to form coordinationinsertion sites in situ to catalyze alkene chain growth cycles, and thus guide future efforts to design Ni-based inorganic porous catalysts and Ni-MOFs.

Isomerization within linear alkenes form mixtures of terminal and internal alkenes and is mediated by primary and secondary reaction pathways on Ni active sites and on residual H⁺ sites. The mechanistic details of the coordination-insertion cycle indicate that selectivity is dictated by kinetic control and thus can be tuned towards terminal alkene products by altering reaction conditions, such as the alkene pressure and presence of intraporous liquid-like alkene phases. Although non-catalytic co-cations are suggested to influence the isomerization of linear alkenes via electronic effects, ⁹⁶ the reported results are inconsistent among alkenes with varying chain lengths. Further

Mini review

experimental and computational studies to examine the effects of alkene chain length, of other extra-framework cations, and of possible chain transfer termination steps to solvents or intrapore condensed hydrocarbons, will improve our current mechanistic understanding of these topics.

Non-catalytic co-cations have also been shown to tune selectivity towards linear oligomers by enhancing steric constraints in inorganic microporous supports, but not in mesoporous supports. The absence of such effects in mesoporous supports is rationalized by lack of proximity between the co-cations and Ni active sites that attenuate the induced electronic effects hypothesized to influence branching in oligomer products. A systematic assessment of the size and shape of the inorganic hosts on isomer selectivity in alkene chain growth reactions is required to understand the effects of steric constraints. Similarly, experimental and computational studies should clarify the possible electronic effects of noncatalytic co-cations that alter coordination-insertion sequences on Ni active sites (Scheme 9) to influence isomer selectivity. Similar to inorganic porous catalysts, Ni-MOFs are generally more selective towards dimerization products than higher oligomers. A few Ni-MOFs,87 however, show comparable selectivities for dimer and higher oligomer products, and selectivity is also shown to be altered by modifying the Ni-MOF structural composition. 100 Mechanistic understanding regarding the dependence of product selectivity on the type of cocatalyst⁸⁷ and solvent used is unclear. Thus, further research is needed to establish relationships between Ni-MOF structural composition and the product selectivity under a standard set of reaction conditions, and to determine the effects of co-catalyst and solvent used. Finally, Ni-MOFs have been predominantly studied for chain growth reactions of ethene, and these systems should also be explored for longer alkenes.

In summary, alkene chain growth reactions catalyzed by heterogeneous porous Ni catalysts are characterized by *in situ* formation of Ni active sites which manifest as activation phenomena. Reaction rates are influenced by the kinetics of the elementary steps involved in the coordination-insertion mechanism, with primary product selectivities governed by the relative rates of these elementary steps. Catalyst lifetime is influenced by the various mechanisms that appear to inhibit and deactivate Ni active sites under reaction conditions. Therefore, improved understanding of the mechanistic aspects underlying these phenomena will help design new material compositions and structures for potential use in practical processes to upgrade biomass- and shale-derived light alkenes into chemical intermediates and transportation fuels.

Conflicts of interest

There are no conflicts to declare.

Acknowledgements

Acknowledgment is made to the donors of the American Chemical Society Petroleum Research Fund for partial support

of this research, under Grant No. 54216-DNI5. This work was also supported in part by the National Science Foundation under Cooperative Agreement No. EEC-1647722, an Engineering Research Center for the Innovative and Strategic Transformation of Alkane Resources.

Research Biographies

Ravi Joshi received his B.S. in Chemical Engineering from the Institute of Chemical Technology (Mumbai, India) in 2013 and his Ph.D. in Chemical Engineering from Purdue University (West Lafayette, USA) in 2019, completing a dissertation titled "Mechanistic Investigations of Ethene Dimerization and Oligomerization Catalyzed by Nickel-Containing Zeotypes".



Arunima Saxena is currently pursuing her Ph.D. in Chemical Engineering at Purdue University (West Lafayette, USA). She received her B. Tech. in Chemical Engineering from the SV National Institute of Technology (Surat, India) in 2017. Her current research focuses on studying Ni-zeolites for alkene oligomerization.



Rajamani Gounder received his B.S. in Chemical Engineering with a double major in Chemistry at the University of Wisconsin (Madison, USA), a Ph.D. in Chemical Engineering at the University of California, Berkeley (Berkeley, USA), and completed postdoctoral research at the California Institute of Technology (Pasadena, USA). In 2013, he started his independent scientific career at Purdue University (West Lafayette, USA), where he currently holds the title of Larry and Virginia Faith Associate Professor in the Davidson School of Chemical Engineering. He leads a research group that is

recognized for studying the kinetic and mechanistic details of catalytic reactions, for synthesizing and designing zeolites and porous materials with tailored site and surface properties, and for developing methods to characterize and titrate active sites in catalytic surfaces. His group studies the catalysis of energy and the environment, focusing on converting conventional and emerging carbon feedstocks to fuels and chemicals, and automotive pollution abatement. His research group has published more than 60 research papers on topics related to catalysis science and technology.



References

- 1. C. O'Connor and M. Kojima, *Catal. Today*, 1990, **6**, 329-349.
- A. Finiels, F. Fajula and V. Hulea, Catal. Sci. Technol., 2014, 4, 2412-2426.
- 3. V. Hulea, ACS Catal., 2018, 8, 3263-3279.
- P. C. A. Bruijnincx and B. M. Weckhuysen, *Angew. Chem. Int. Ed.*, 2013, **52**, 11980-11987.
- N. M. Eagan, M. D. Kumbhalkar, J. S. Buchanan, J. A. Dumesic and G. W. Huber, *Nature Reviews Chemistry*, 2019, 3, 223-249.
- 6. K. Ziegler, Brennst.-Chem, 1954, 35, 321.
- 7. K. Fischer, K. Jonas, P. Misbach, R. Stabba and G. n. Wilke, *Angew. Chem. Int. Ed. Engl.*, 1973, **12**, 943-953.
- 8. W. Keim, Angew. Chem. Int. Ed. Engl., 1990, 29, 235-244.
- 9. F. Speiser, P. Braunstein and L. Saussine, *Acc. Chem. Res.*, 2005, **38**, 784-793.
- 10. C. T. O'Connor and M. Kojima, *Catal. Today*, 1990, **6**, 329-349.
- 11. J. Skupinska, Chem. Rev., 1991, 91, 613-648.
- 12. D. S. McGuinness, *Chem. Rev.*, 2011, **111**, 2321-2341.
- 13. B. L. Small, Acc. Chem. Res., 2015, 48, 2599-2611.
- 14. C. P. Nicholas, App. Catal., A, 2017, 543, 82-97.
- A. Kermagoret and P. Braunstein, Organometallics, 2008, 27, 88-99.
- 16. S. Forget, H. Olivier-Bourbigou and D. Delcroix, *ChemCatChem*, 2017, **9**, 2408-2417.
- 17. P. Braunstein and F. Naud, *Angew. Chem. Int. Ed.*, 2001, **40**, 680-699.
- 18. U. Rosenthal, B. H. Müller, N. Peulecke, S. Peitz, A. Wöhl, W. Müller, H. Olivier-Bourbigou, L. Magna, P. W. N. M. van Leeuwen, M. J. L. Tschan, M. Hapke, N. Weding and K. Kral, in Applied Homogeneous Catalysis with Organometallic Compounds, Wiley-VCH Verlag GmbH & Co. KGaA, 2017, DOI: 10.1002/9783527651733.ch5, pp. 307-410.

- 19. Y. Chauvin, J. Gaillard, D. V. Quang and J. Andrews, *Chemistry & Industry*, 1974, 375-378.
- 20. D. Vogt, in *Aqueous-Phase Organometallic Catalysis*, Wiley-VCH Verlag GmbH & Co. KGaA, 2005, DOI: 10.1002/3527602488.ch7a, pp. 637-654.
- 21. A. Forestière, H. Olivier-Bourbigou and L. Saussine, *Oil & Gas Science and Technology Rev. IFP*, 2009, **64**, 649-667.
- 22. S. Tabak, F. Krambeck and W. Garwood, *AIChE journal*, 1986, **32**, 1526-1531.
- 23. M. L. Sarazen and E. Iglesia, *Proceedings of the National Academy of Sciences*, 2017, **114**, E3900-E3908.
- S. Svelle, S. Kolboe and O. Swang, J. Phys. Chem. B, 2004, 108, 2953-2962.
- 25. M. Aronson, R. Gorte and W. E. Farneth, *J. Catal.*, 1986, **98**, 434-443.
- H. Olivier-Bourbigou, P. A. R. Breuil, L. Magna, T. Michel, M. F. Espada Pastor and D. Delcroix, *Chem. Rev.*, 2020, DOI: 10.1021/acs.chemrev.0c00076.
- 27. P. Cossee, Tetrahedron Lett., 1960, 1, 12-16.
- 28. P. Cossee, J. Catal., 1964, 3, 80-88.
- 29. E. J. Arlman and P. Cossee, J. Catal., 1964, 3, 99-104.
- 30. R. H. Grubbs and A. Miyashita, *J. Chem. Soc., Chem. Commun.*, 1977, 864-865.
- 31. R. H. Grubbs and A. Miyashita, *J. Am. Chem. Soc.*, 1978, **100**, 7416-7418.
- 32. W. Keim, Angew. Chem. Int. Ed., 2013, 52, 12492-12496.
- 33. R. Joshi, G. Zhang, J. T. Miller and R. Gounder, *ACS Catal.*, 2018, **8**, 11407-11422.
- 34. S. D. Ittel, L. K. Johnson and M. Brookhart, *Chem. Rev.*, 2000, **100**, 1169-1204.
- 35. G. J. P. Britovsek, V. C. Gibson and D. F. Wass, *Angew. Chem. Int. Ed.*, 1999, **38**, 428-447.
- 36. P. Kuhn, D. Sémeril, D. Matt, M. J. Chetcuti and P. Lutz, *Dalton Transactions*, 2007, DOI: 10.1039/B615259G, 515-528.
- 37. M. A. Escobar, O. S. Trofymchuk, B. E. Rodriguez, C. Lopez-Lira, R. Tapia, C. Daniliuc, H. Berke, F. M. Nachtigall, L. S. Santos and R. S. Rojas, *ACS Catal.*, 2015, **5**, 7338-7342.
- 38. R. Y. Brogaard and U. Olsbye, ACS Catal., 2016, 6, 1205-1214.
- 39. A. K. Ghosh and L. Kevan, J. Phys. Chem., 1990, 94, 3117-3121.
- 40. I. V. Elev, *J. Catal.*, 1984, **89**, 470-477.
- 41. M. Hartmann, A. Pöppl and L. Kevan, *J. Phys. Chem.*, 1996, **100**, 9906-9910.
- 42. L. Bonneviot, D. Olivier and M. Che, *J. Mol. Catal.*, 1983, **21**, 415-430.
- 43. H. Choo and L. Kevan, J. Phys. Chem. B, 2001, 105, 6353-6360.
- 44. Z. Chang, Z. Zhu and L. Kevan, J. Phys. Chem. B, 1999, **103**, 9442-9449.
- 45. J. Krzystek, J.-H. Park, M. W. Meisel, M. A. Hitchman, H. Stratemeier, L.-C. Brunel and J. Telser, *Inorganic chemistry*, 2002, **41**, 4478-4487.
- 46. A. Martínez, M. A. Arribas, P. Concepción and S. Moussa, *App. Catal.*, *A*, 2013, **467**, 509-518.
- 47. R. Henry, M. Komurcu, Y. Ganjkhanlou, R. Y. Brogaard, L. Lu, K. J. Jens, G. Berlier and U. Olsbye, *Catal. Today*, 2018, **299**, 154-163.
- 48. M. Lallemand, A. Finiels, F. Fajula and V. Hulea, *J. Phys. Chem. C*, 2009, **113**, 20360-20364.
- 49. A. N. Mlinar, G. B. Baur, G. G. Bong, A. B. Getsoian and A. T. Bell, *J. Catal.*, 2012, **296**, 156-164.
- S. A. Svejda and M. Brookhart, Organometallics, 1999, 18, 65-74.

- 51. S. A. Svejda, L. K. Johnson and M. Brookhart, *J. Am. Chem. Soc.*, 1999, **121**, 10634-10635.
- 52. E. D. Metzger, C. K. Brozek, R. J. Comito and M. Dincă, ACS Central Science, 2016, 2, 148-153.
- 53. E. D. Metzger, R. J. Comito, C. H. Hendon and M. Dincă, *J. Am. Chem. Soc.*, 2017, **139**, 757-762.
- 54. S. Moussa, P. Concepción, M. A. Arribas and A. Martínez, *ACS Catal.*, 2018, **8**, 3903-3912.
- 55. A. Ehrmaier, Y. Liu, S. Peitz, A. Jentys, Y.-H. C. Chin, M. Sanchez-Sanchez, R. Bermejo-Deval and J. Lercher, *ACS Catal.*, 2019, **9**, 315-324.
- 56. I. Agirrezabal-Telleria and E. Iglesia, *J. Catal.*, 2017, **352**, 505-514.
- 57. I. Agirrezabal-Telleria and E. Iglesia, *J. Catal.*, 2020, **389**, 690-705.
- R. Y. Brogaard, M. Kømurcu, M. Dyballa, A. Botan, V. Van Speybroeck, U. Olsbye and K. De Wispelaere, ACS Catal., 2019, 9, 5645-5650.
- 59. P. Kuhn, D. Semeril, D. Matt, M. J. Chetcuti and P. Lutz, *Dalton Transactions*, 2007, DOI: 10.1039/B615259G, 515-528.
- 60. R. J. Comito, E. D. Metzger, Z. Wu, G. Zhang, C. H. Hendon, J. T. Miller and M. Dincă, *Organometallics*, 2017, **36**, 1681-1683.
- 61. S. T. Madrahimov, J. R. Gallagher, G. Zhang, Z. Meinhart, S. J. Garibay, M. Delferro, J. T. Miller, O. K. Farha, J. T. Hupp and S. T. Nguyen, *ACS Catal.*, 2015, **5**, 6713-6718.
- 62. J. Canivet, S. Aguado, Y. Schuurman and D. Farrusseng, *J. Am. Chem. Soc.*, 2013, **135**, 4195-4198.
- 63. V. Bernales, A. B. League, Z. Li, N. M. Schweitzer, A. W. Peters, R. K. Carlson, J. T. Hupp, C. J. Cramer, O. K. Farha and L. Gagliardi, *J. Phys. Chem. C*, 2016, **120**, 23576-23583.
- 64. B. Liu, S. Jie, Z. Bu and B.-G. Li, *RSC Advances*, 2014, **4**, 62343-62346.
- Z. Li, N. M. Schweitzer, A. B. League, V. Bernales, A. W. Peters,
 A. B. Getsoian, T. C. Wang, J. T. Miller, A. Vjunov, J. L. Fulton,
 J. A. Lercher, C. J. Cramer, L. Gagliardi, J. T. Hupp and O. K.
 Farha, J. Am. Chem. Soc., 2016, 138, 1977-1982.
- 66. E. Zurek and T. Ziegler, *Progress in Polymer Science*, 2004, **29**, 107-148.
- 67. J. J. Eisch, in *Comprehensive Organometallic Chemistry II*, eds. E. W. Abel, F. G. A. Stone and G. Wilkinson, Elsevier, Oxford, 1995, pp. 431-502.
- 68. M. Linnolahti and S. Collins, *ChemPhysChem*, 2017, **18**, 3369-
- 69. M. Bochmann, Organometallics, 2010, 29, 4711-4740.
- 70. E. Y.-X. Chen and T. J. Marks, *Chem. Rev.*, 2000, **100**, 1391-
- 71. J. J. Eisch, S. I. Pombrik and G. X. Zheng, *Organometallics*, 1993, **12**, 3856-3863.
- A. N. Mlinar, B. K. Keitz, D. Gygi, E. D. Bloch, J. R. Long and A. T. Bell, ACS Catal., 2014, DOI: 10.1021/cs401189a, 717-721.
- 73. M. Kømurcu, A. Lazzarini, G. Kaur, E. Borfecchia, S. Øien-Ødegaard, D. Gianolio, S. Bordiga, K. P. Lillerud and U. Olsbye, *Catal. Today*, 2020, DOI: 10.1016/j.cattod.2020.03.038.
- 74. J. Heveling, A. van der Beek and M. de Pender, *App. Catal.*, 1988, **42**, 325-336.
- 75. F. T. T. Ng and D. C. Creaser, in *Stud. Surf. Sci. Catal.*, eds. J. S. Kevin and C. S. Emerson, Elsevier, 1992, vol. Volume 73, pp. 123-131.
- 76. M. Lallemand, O. A. Rusu, E. Dumitriu, A. Finiels, F. Fajula and V. Hulea, *App. Catal., A*, 2008, **338**, 37-43.
- A. N. Mlinar, S. Shylesh, O. C. Ho and A. T. Bell, ACS Catal., 2014, 4, 337-343.

- R. D. Andrei, M. I. Popa, F. Fajula and V. Hulea, J. Catal., 2015, 323, 76-84.
- 79. Y. Ganjkhanlou, G. Berlier, E. Groppo, E. Borfecchia and S. Bordiga, *Top. Catal.*, 2017, **60**, 1664-1672.
- 80. A. Brückner, U. Bentrup, H. Zanthoff and D. Maschmeyer, *J. Catal.*, 2009, **266**, 120-128.
- 81. V. Hulea and F. Fajula, J. Catal., 2004, 225, 213-222.
- 82. J. F. Haw, W. Song, D. M. Marcus and J. B. Nicholas, *Acc. Chem. Res.*, 2003, **36**, 317-326.
- 83. U. Olsbye, M. Bjørgen, S. Svelle, K.-P. Lillerud and S. Kolboe, *Catal. Today*, 2005, **106**, 108-111.
- 84. M. Lallemand, A. Finiels, F. Fajula and V. Hulea, *App. Catal., A*, 2006, **301**, 196-201.
- 85. Y. T. Kim, J. P. Chada, Z. Xu, Y. J. Pagan-Torres, D. C. Rosenfeld, W. L. Winniford, E. Schmidt and G. W. Huber, *J. Catal.*, 2015, **323**. 33-44.
- 86. R. J. Davis, in *Catalysis for the Conversion of Biomass and Its Derivatives*, Max Planck Research Library for the History and Development of Knowledge, Berlin, Germany, Open Access edn., 2013, p. 262.
- 87. L. Chen, Y. Jiang, H. Huo, J. Liu, Y. Li, C. Li, N. Zhang and J. Wang, *App. Catal.*, *A*, 2020, **594**, 117457.
- 88. E. D. Metzger, R. J. Comito, Z. Wu, G. Zhang, R. C. Dubey, W. Xu, J. T. Miller and M. Dincă, *ACS Sustainable Chemistry & Engineering*, 2019, **7**, 6654-6661.
- 89. M. Sanati, C. Hornell and S. G. Jaras, in *Catalysis*, The Royal Society of Chemistry, Cambridge, 1999, vol. 14, p. 236.
- R. J. Quann, L. A. Green, S. A. Tabak and F. J. Krambeck, *Ind. Eng. Chem. Res.*, 1988, 27, 565-570.
- 91. D. B. Lukyanov, N. S. Gnep and M. R. Guisnet, *Ind. Eng. Chem. Res.*, 1994, **33**, 223-234.
- 92. S. Moussa, M. A. Arribas, P. Concepción and A. Martínez, *Catal. Today*, 2016, **277**, 78-88.
- 93. M. I. Gonzalez, J. Oktawiec and J. R. Long, *Faraday Discussions*, 2017, **201**, 351-367.
- 94. U. S. F. Arrozi, V. Bon, C. Kutzscher, I. Senkovska and S. Kaskel, *Dalton Transactions*, 2019, **48**, 3415-3421.
- A. N. Mlinar, O. C. Ho, G. G. Bong and A. T. Bell, *ChemCatChem*, 2013, 5, 3139-3147.
- 96. A. Ehrmaier, S. Peitz, M. Sanchez-Sanchez, R. Bermejo-Deval and J. Lercher, *Microporous Mesoporous Mater.*, 2019, **284**, 241-246.
- 97. K. Ziegler, E. Holzkamp, H. Breil and H. Martin, *Angewandte Chemie*, 1955, **67**, 426-426.
- 98. D. Vogt, in *Applied homogeneous catalysis with organometallic compounds: a comprehensive handbook [2nd. ed.]*, Wiley-VCH Verlag, 2002, pp. 240-253.
- 99. G. J. P. Britovsek, R. Malinowski, D. S. McGuinness, J. D. Nobbs, A. K. Tomov, A. W. Wadsley and C. T. Young, *ACS Catal.*, 2015, 5, 6922-6925.
- J. Liu, J. Ye, Z. Li, K.-i. Otake, Y. Liao, A. W. Peters, H. Noh,
 D. G. Truhlar, L. Gagliardi, C. J. Cramer, O. K. Farha and J. T.
 Hupp, J. Am. Chem. Soc., 2018, 140, 11174-11178.
- M. D. Heydenrych, C. P. Nicolaides and M. S. Scurrell, J. Catal., 2001, 197, 49-57.